Monthly Notices
of the
ROYAL ASTRONOMICAL SOCIETY

MNRAS **469,** 2121–2140 (2017)
Advance Access publication 2017 April 1

doi:10.1093/mnras/stx808

The mass–metallicity relation revisited with CALIFA

S. F. Sánchez,[1⋆] J. K. Barrera-Ballesteros,[2⋆] L. Sánchez-Menguiano,[3,4⋆] C. J. Walcher,[5] R. A. Marino,[6] L. Galbany,[7] J. Bland-Hawthorn,[8] M. Cano-Díaz,[1] R. García-Benito,[3] C. López-Cobá,[1] S. Zibetti,[9] J. M. Vilchez,[3] J. Iglésias-Páramo,[3] C. Kehrig,[3] A. R. López Sánchez,[10,11] S. Duarte Puertas[3] and B. Ziegler[12]

[1]*Instituto de Astronomía, Universidad Nacional Autónoma de México, A. P. 70-264, C.P. 04510 México, D.F., Mexico*
[2]*Department of Physics & Astronomy, Johns Hopkins University, Bloomberg Center, 3400 N. Charles St, Baltimore, MD 21218, USA*
[3]*Instituto de Astrofísica de Andalucía (IAA/CSIC), Glorieta de la Astronomía s/n Aptdo. 3004, E-18080 Granada, Spain*
[4]*Departamento de Física Teórica y del Cosmos, University of Granada, Facultad de Ciencias (Edificio Mecenas), E-18071 Granada, Spain*
[5]*Leibniz-Institut für Astrophysik Potsdam (AIP), An der Sternwarte 16, D-14482 Potsdam, Germany*
[6]*Department of Physics, Institute for Astronomy, ETH Zürich, CH-8093 Zürich, Switzerland*
[7]*PITT PACC, Department of Physics and Astronomy, University of Pittsburgh, Pittsburgh, PA 15260, USA*
[8]*Sydney Institute for Astronomy, School of Physics, University of Sydney, NSW 2006, Australia*
[9]*INAF-Osservatorio Astrofisico di Arcetri – Largo Enrico Fermi, 5 – I-50125 Firenze, Italy*
[10]*Australian Astronomical Observatory, PO Box 915, North Ryde, NSW 1670, Australia*
[11]*Department of Physics and Astronomy, Macquarie University, NSW 2109, Australia*
[12]*Department of Astrophysics, University of Vienna, Türkenschanzstr 17, A-1180 Vienna, Austria*

Accepted 2017 March 30. Received 2017 March 29; in original form 2017 February 10

ABSTRACT

We present an updated version of the mass–metallicity (MZ) relation using integral field spectroscopy data obtained from 734 galaxies observed by the CALIFA survey. These unparalleled spatially resolved spectroscopic data allow us to determine the metallicity at the same physical scale (R_e) for different calibrators. We obtain MZ relations with similar shapes for all calibrators, once the scalefactors among them are taken into account. We do not find any significant secondary relation of the MZ relation with either the star formation rate (SFR) or the specific SFR for any of the calibrators used in this study, based on the analysis of the residuals of the best-fitted relation. However, we do see a hint for an (s)SFR-dependent deviation of the MZ relation at low masses ($M < 10^{9.5}$ $M_\odot$), where our sample is not complete. We are thus unable to confirm the results by Mannucci et al. (2010), although we cannot exclude that this result is due to the differences in the analysed data sets. In contrast, our results are inconsistent with the results by Lara-López et al. (2010), and we can exclude the presence of an SFR–mass–oxygen abundance fundamental plane. These results agree with previous findings suggesting that either (1) the secondary relation with the SFR could be induced by an aperture effect in single fibre/aperture spectroscopic surveys, (2) it could be related to a local effect confined to the central regions of galaxies or (3) it is just restricted to the low-mass regime, or a combination of the three effects.

Key words: techniques: spectroscopic – galaxies: abundances – galaxies: evolution – galaxies: ISM.

1 INTRODUCTION

Galaxies in the Local Universe are perfect laboratories for the study of the star formation and chemical enrichment history. Their spectroscopic properties retain the fossil records of cosmological evolution. For that reason, they possess correlations between their different properties that are a consequence of that evolution, like the so-called star formation main sequence (SFMS, e.g. Brinchmann et al. 2004) or the mass–metallicity (MZ) relations. Those correlations change with cosmological time tracing the evolution of the stellar populations (e.g. Davé, Oppenheimer & Finlator 2011).

The MZ relation determined from emission-line diagnostics was formally presented by Tremonti et al. (2004, T04 hereafter), although the correlation appears in different forms in the earlier

⋆ E-mail: sfsanchez@astro.unam.mx (SFS); jbarrer3@jh.edu (JKB-B); lsanchez@iaa.es (LS-M)

literature going back several decades (e.g. Lequeux et al. 1979; Garnett & Shields 1987; Vila-Costas & Edmunds 1992). The MZ relation exhibits a strong correlation between the stellar mass and the average oxygen abundance in galaxies. Derived for a few tens of thousands of galaxies observed by the SDSS survey, it extends over four order of magnitudes in mass and presents a small dispersion [$\sigma_{\log(O/H)} \sim 0.1$ dex]. This correlation has been confirmed at different redshifts, showing a clear evolution with cosmological time, as a result of the increase of the stellar mass and the oxygen enrichment (e.g. Erb et al. 2006; Erb 2008; Henry et al. 2013; Maier et al. 2014, 2015; Saviane et al. 2014; Salim et al. 2015; Maier et al. 2016). Its functional form may depend on the adopted abundance calibrator (e.g. Kewley & Ellison 2008). However, it is rather stable when using single-aperture spectroscopic data or spatial resolved information (e.g. Rosales-Ortega et al. 2012a; Sánchez et al. 2014). Despite the differences in methodology and physical interpretation, a similar relation has been reported for the metallicity of stellar populations (e.g. Gallazzi et al. 2005; González Delgado et al. 2014b).

The original interpretation of the shape of this relation (T04), with its clear saturation in the abundance at high stellar mass, was that galactic outflows regulate the metal content. The idea here is that outflows are more efficient for larger star formation rates (SFRs) presumed to occur in higher mass galaxies. This interpretation was re-phrased recently by Belfiore, Maiolino & Bothwell (2016) indicating that galaxies reach an equilibrium metallicity in which the metals expelled by outflows are compensated by those produced by star formation. However, this interpretation requires that the outflows are strong enough to escape the gravitational potential and expel a substantial fraction of the generated oxygen, overcoming the effect of 'rainfall' and metal mixing. Rosales-Ortega et al. (2012a) presented an alternative explanation in which the effect of outflows is not required. They show that the integrated relation is easily derived from a new, *more fundamental* relation between the stellar mass density and the local oxygen abundance. This relation was confirmed with larger statistics by Sánchez et al. (2013) and more recently by Barrera-Ballesteros et al. (2016), using MaNGA data (Bundy et al. 2015). Under the proposed scenario, the stellar mass growth and the metal enrichment are both dominated by local processes, basically the *in situ* star formation, with little influence of outflows or radial migrations. The differential star formation history from the inner to the outer regions, known as local downsizing (e.g. Pérez et al. 2013; Ibarra-Medel et al. 2016), and the fact that oxygen enrichment is directly coupled with star formation explain both the local and the global MZ relations naturally. Moreover, the local relation explains the oxygen abundance gradients observed in galaxies (e.g. Sánchez et al. 2015), as recently shown by Barrera-Ballesteros et al. (2016). Under this assumption, the plateau reached in the MZ relation is a pure consequence of the maximum yield of oxygen abundance and a characteristic depletion time, as already suggested by Pilyugin, Thuan & Vílchez (2007).

On the other hand, Mannucci et al. (2010) and Lara-López et al. (2010) presented almost simultaneously an analysis of the dependence of the MZ relation with the SFR, that they called fundamental mass–metallicity relation (FMR), in the first case, and SFR–mass–oxygen abundance fundamental plane (FP), in the second case. They both showed that there is a secondary relation in the sense that, at a fixed stellar mass, galaxies with stronger SFR exhibit lower oxygen abundances (a result that was previously reported by Ellison et al. 2008). Although the adopted functional form for this secondary relation was different in both studies, the conclusions were very similar. That correlation is a bit anti-intuitive, since oxygen abundance is enhanced due to star formation. Both studies were based on two similar sub-samples of the same observational data set. They both used the SDSS spectroscopic survey at $z \sim 0.1$ (from which the oxygen abundance and the star formation were derived) combined with the photometric information to derive the integrated stellar mass. They applied aperture corrections to the SFR (Brinchmann et al. 2004), due to the strong aperture effects of the SDSS single fibre spectroscopic information (e.g. Iglesias-Páramo et al. 2013; Gomes et al. 2016). However, they did not apply any aperture correction to oxygen abundance indicators, what could be substantially important (e.g. Iglesias-Páramo et al. 2016). Even more, the applied corrections depend on certain correlations between the SFR and the colour gradients in galaxies, which are not fully tested. Recent results indicate that those corrections could be strongly affected by the assumed correlations (Duarte Puertas et al. 2017).

This result is under discussion. Sánchez et al. (2013) showed that using catalogue of H II regions extracted from the CALIFA data set (Sánchez et al. 2012) observed up to that date (150 galaxies), the secondary relation cannot be confirmed. In a contemporary article, Hughes et al. (2013) have shown that using drift-scan integrated spectra the secondary relation is not present. Indeed, Rosales-Ortega et al. (2012a) had already shown that the relation with the specific star formation rate [sSFR, in the form of the EW(H α)] of the local MZ relation does not present a secondary trend, following the primary relation between the SFR and the mass, as studied in detail in Sánchez et al. (2013). Actually, T04 explored the residuals of the MZ relation, and found that there was no evidence for a relation with the EW(H α). A different approach was presented by Salim et al. (2014). In this case, they analysed the SDSS data exploring the relation between the oxygen abundance and the sSFR for different mass bins. They found a clear anticorrelation but considerably weaker than the one presented by Mannucci et al. (2010) and Lara-López et al. (2010). They repeated the analysis using the CALIFA data presented by Sánchez et al. (2013), finding a similar result (i.e. that there is a secondary correlation).

Furthermore, Moran et al. (2012) showed that the secondary relation is not seen in their data, and they proposed a secondary relation with the gas fraction as previously explored by Vila-Costas & Edmunds (1992). In the same line, Bothwell et al. (2016) shows that the primary driver for the FMR is the relation between SFR and molecular gas (Kennicutt, Keel & Blaha 1989), in their analysis of a sample covering a wide range of redshifts ($0 < z < 2$). They found a clear trend between the residual of the MZ relation and the molecular gas mass (fig. 4 of that article). However, in a previous article exploring galaxies in a much narrower redshift range at the Local Universe, Bothwell et al. (2013) shown that while there is secondary relation of the MZ relation with the atomic cold gas (H I), they cannot confirm the existence of a secondary relation with the molecular gas (H2). Since atomic gas is not a tracer of the SFR that secondary relation would imply a new, different relation than the proposed FMR, in agreement with the results presented by Moran et al. (2012), described before. Therefore, the presence of secondary relation with the molecular gas mass, the tracer of the SFR, is under discussion, even more if it is considered the strong correlation between the CO/H_2 correction factor with the metallicity (e.g. Bolatto, Wolfire & Leroy 2013), as already pointed out by Bothwell et al. (2013).

Furthermore, recent results have shown that even using single-aperture spectroscopic data the secondary relation between the MZ and the SFR may disappear when using particular abundance calibrators (e.g. Kashino et al. 2016). And, in any case, it seems

to be weaker than what it was previously reported (e.g. Telford et al. 2016), and strongly dependent on the assumptions behind the derivation of the three parameters involved: for example, the SFR derivation is based on calibrations that assume solar abundances (e.g. Kennicutt et al. 1989). Finally, in a complementary study presented by Barrera-Ballesteros et al. (2017), it is not found any secondary correlation with the SFR based on the analysis of the sample of galaxies observed by the MaNGA survey (Bundy et al. 2015) up to date.

In the current article, we revisit the MZ relation and its possible dependence with the SFR using the integral field spectroscopic data provided by the full sample of galaxies observed by the CALIFA survey (Sánchez et al. 2012). The distribution of the article is as follows: in Section 2, we present the sample of galaxies and the adopted data set; the adopted calibrators to derive the oxygen abundance are described in Section 3.1; in Section 4.1, we present the MZ relation derived using these data, and the possible dependence with the SFR is explored in Section 4.2; a comparison with the so-called FMR is included in Section 4.3, and the possible dependence of the residuals of the MZ relation with either the sSFR or the residual of the SFMS are explored in Section 4.5; finally the results are discussed in Section 5.

2 SAMPLE AND DATA

The analysed sample comprises all the galaxies with good quality spectroscopic data observed with the low resolution setup (V500) by the CALIFA survey (Sánchez et al. 2012) and by a number of CALIFA-extensions listed in Sánchez et al. (2016c) up to 2016 October 9. It includes the 667 galaxies from the 3rd CALIFA Data Release (Sánchez et al. 2016c), and in addition we include those galaxies with good quality data excluded from DR3 because either they did not have SDSS-DR7 imaging data (a primary selection for DR3) or they were observed after the final sample was closed (i.e. after 2015 November). The final sample comprises a total of 734 galaxies.

The main properties of this sample are shown in Fig. 1, including the redshift, effective radius and $B-R$ colour distribution along the absolute magnitude of the galaxies. All the parameters were derived directly from the data cubes. The redshift was derived as part of the PIPE3D analysis described later. The photometric parameters were extracted from the data cubes by convolving the Johnson filter responses and applying the zero-points listed in Fukugita, Shimasaku & Ichikawa (1995). For comparison purposes, we have included the same properties for the galaxies observed by the MaNGA (Bundy et al. 2015) and SAMI (Croom et al. 2012) surveys. For clarifying purposes and prior to any further analysis, we find interesting to include this comparison due to the similar goals of the three surveys, that can lead to the analysis of the current topic using the three data sets (already performed by Barrera-Ballesteros et al. (2017) with MaNGA data). For MaNGA, we used the published sample included in the SDSS-DR13 (the so-called MPL-4 data set, SDSS Collaboration et al. 2016). For SAMI, we used the catalogue of galaxies observed up to summer 2016. The figure shows that the analysed sample covers a much narrower range of redshifts, offers a better physical resolution per galaxy and covers a similar range of absolute magnitudes, colours and effective radius, than that of the other two major Integral Field Unit (IFU) surveys. On one hand, MaNGA presents a flatter distribution in masses by construction, at the cost of observing the most massive ones at a considerably larger redshift (and lower physical resolution). On the other hand, SAMI samples better the low luminosity/bluer range of the colour–magnitude diagram. This is already known for the CALIFA Mother Sample, that it is not complete below $10^{9-9.5}$ $M_{\odot}$ (e.g. Walcher et al. 2014). However, the analysed sample is more similar to the CALIFA DR3 sample (Sánchez et al. 2016c), covering better the lower mass/luminosity range of the colour–magnitude diagram, and being more suitable for the proposed exploration, due to the inclusion of the CALIFA-extended samples.

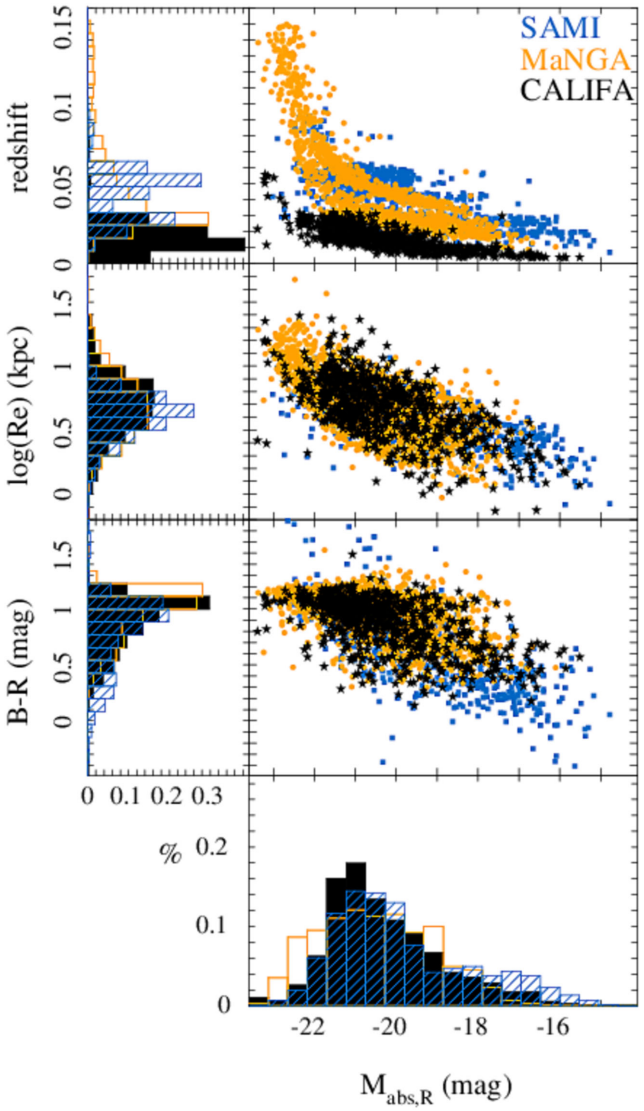

Figure 1. Comparison of the main properties of the analysed sample (CALIFA) with that of similar samples observed by current on-going IFU surveys (MaNGA, SAMI). The plot shows the redshift, effective radius and colour distributions along the absolute magnitudes, together with the corresponding frequency histograms for the current analysed sample (black stars), the MaNGA sample distributed in the SDSS-DR13 (MPL-4 sample), and the SAMI sample observed up to summer 2016.

The details of the CALIFA survey, including the observational strategy and data reduction are explained in Sánchez et al. (2012, 2016c). All galaxies were observed using PMAS (Roth et al. 2005) in the PPaK configuration (Kelz et al. 2006), covering a hexagonal field of view (FoV) of 74 arcsec × 64 arcsec, which is sufficient to map the full optical extent of the galaxies up to two to three disc effective radii. This is possible because of the diameter selection of the CALIFA sample (Walcher et al. 2014). The

observing strategy guarantees complete coverage of the FoV, with a final spatial resolution of full width at half-maximum ∼2.5 arcsec, corresponding to ∼1 kpc at the average redshift of the survey (e.g. García-Benito et al. 2015; Sánchez et al. 2016c). The sampled wavelength range and spectroscopic resolution for the adopted setup (3745–7500 Å, $\lambda/\Delta\lambda \sim 850$, V500 setup) are more than sufficient to explore the most prominent ionized gas emission lines from [O II] λ3727 to [S II] λ6731 at the redshift of our targets, on one hand, and to deblend and subtract the underlying stellar population, on the other (e.g. Kehrig et al. 2012; Cid Fernandes et al. 2013, 2014; Sánchez et al. 2013, 2014, 2016a). In addition, most of the objects are observed using a higher resolution setup, covering only the blue end of the spectral range (3700–4800 Å, $\lambda/\Delta\lambda \sim 1650$, V1200 setup), that it is not used in the current analysis. The current data set was reduced using version 2.2 of the CALIFA pipeline, whose modifications with respect to the previous ones (Sánchez et al. 2012; Husemann et al. 2013; García-Benito et al. 2015) are described in Sánchez et al. (2016c). The final dataproduct of the reduction is a data cube comprising the spatial information in the *x*- and *y*-axis, and the spectral one in the *z* one. For further details of the adopted dataformat and the quality of the data, consult Sánchez et al. (2016c).

3 ANALYSIS

We analyse the data cubes using the PIPE3D pipeline (Sánchez et al. 2016b), which is designed to fit the continuum with stellar population models and measure the nebular emission lines of IFS data. This pipeline is based on the FIT3D fitting package (Sánchez et al. 2016a). The current implementation of PIPE3D adopts the GSD156 library of simple stellar populations (Cid Fernandes et al. 2013), that comprises 156 templates covering 39 stellar ages (from 1 Myr to 13 Gyr) and four metallicities ($Z/Z_{\odot} = 0.2$, 0.4, 1 and 1.5). These templates have been extensively used within the CALIFA collaboration (e.g. Pérez et al. 2013; González Delgado et al. 2014a) and for other surveys (e.g. Ibarra-Medel et al. 2016). Details of the fitting procedure, dust attenuation curve and uncertainties of the processing of the stellar populations are given in Sánchez et al. (2016a,b).

In summary, for the stellar population analysis, it is performed a spatial binning to each data cube to reach a goal S/N of 50 across the FoV. Then, the stellar population fitting was applied to the co-added spectra within each spatial bin. Finally, following the procedures described in Cid Fernandes et al. (2013) and Sánchez et al. (2016a), we estimate the stellar-population model for each spaxel by re-scaling the best-fitted model within each spatial bin to the continuum flux intensity in the corresponding spaxel. This model is used to derive the stellar mass density at each position, in a similar way as described in Cano-Díaz et al. (2016), adopting the Salpeter IMF (Salpeter 1955), and then co-added to estimate the integrated stellar mass of the galaxies. That estimation of the stellar mass has a typical error of 0.15 dex, as described in Sánchez et al. (2016b).

The stellar-population model spectra are then subtracted to the original cube to create a gas-pure cube comprising only the ionized gas emission lines (and the noise). Individual emission line fluxes were then measured spaxel by spaxel using both a single Gaussian fitting for each emission line and spectrum, and a weighted momentum analysis, as described in Sánchez et al. (2016b). For this particular data set, we extracted the flux intensity of the following emission lines: H α, H β, [O II] λ3727, [O III] λ4959, [O III] λ5007, [N II] λ6548, [N II] λ6583, [S II]λ6717 and [S II]λ6731. The intensity maps for each of these lines are corrected by dust attenuation, derived using the spaxel-to-spaxel H α/H β ratio. Then it is assumed a canonical value of 2.86 for this ratio (Osterbrock 1989), and adopting a Cardelli, Clayton & Mathis (1989) extinction law and $R_V = 3.1$ (i.e. a Milky Way like extinction law Schlegel, Finkbeiner & Davis 1998).

For the spatial resolved oxygen abundance we select only those spaxels for which ionization is clearly compatible with those being produced by star-forming areas, following Sánchez et al. (2013). For doing so, we select those spaxel located below the Kewley et al. (2001) demarcation curve in the classical BPT diagnostic diagram (Baldwin, Phillips & Terlevich 1981, [O III]/H β versus [N II]/H α diagram), and with a EW(H α) larger than 6 Å. These criteria ensure that the ionization is compatible with being due to young stars (Sánchez et al. 2014), and therefore the abundance calibrators can be applied. The H α luminosity is derived by correcting for the cosmological distance the dust corrected H α intensity maps. Then, by applying the Kennicutt (1998) calibration (for the Salpeter IMF), we derive the spatial resolved distribution of the SFR surface density, and finally the integrated SFR. We did not apply the very restrictive selection criterion indicated before [EW(H α) > 6 Å] for the derivation of the SFR in order to include the diffuse ionized gas. While in retired galaxies (or areas within galaxies) this ionized gas is most probably dominated by post-AGB ionization (e.g. Sarzi et al. 2010; Singh et al. 2013; Gomes et al. 2016), in star-forming galaxies the photon leaking from H II regions may represent a large contribution to the integrated H α luminosity (e.g. Relaño et al. 2012; Morisset et al. 2016), and the SFR estimation. The contamination of the post-AGB ionization in our derivation of SFR represents a contribution more than two orders of magnitude lower than the actual SFR for galaxies located in the SFMS (e.g. Catalán-Torrecilla et al. 2015; Cano-Díaz et al. 2016; Duarte Puertas et al. 2017). Thus, it affects the SFR by less than a ∼1 per cent for those galaxies. For H α, we applied a signal-to-noise cut of 3σ spaxel by spaxel, while for the remaining lines we relax that cut down to 1σ. The cut in H α ensures a positive detection of the ionized gas, while the cut in the other lines limits the error for the derived parameters.

Finally, we determine the oxygen abundance for each spaxel using the different calibrators described in Section 3.1, using the dust extinction corrected intensity maps for the set of emission lines described before, based on the dust extinction correction described before. We adopted as a characteristic oxygen abundance for each galaxy the value derived at the effective radius R_e. This abundance matches pretty well with the average abundance across the optical extension of the galaxies, as demonstrated by Sánchez et al. (2013). To derive this abundance, we perform a linear fitting to the deprojected abundance gradient within a range of galactocentric distances between 0.5 and 2.0 R_e, as described in Sánchez et al. (2013) and Sánchez-Menguiano et al. (2016). This abundance gradient has a nominal error well below the typical error for a single-aperture spectroscopic derivation (Salim et al. 2014) due to the larger number of sampled points for each single galaxy, being typically ∼0.03 dex (e.g. Sánchez et al. 2013). The photometric properties of the galaxies (stellar mass [$M_{\odot}$], PA and ellipticity) were obtained from CALIFA DR3 tables,[1] derived as described in Walcher et al. (2014). We use as final sample those galaxies where it is possible to determine the oxygen abundance at the R_e fulfilling the above criteria (612 objects). Fig. 2 shows the comparison between the average oxygen abundance derived using all the suitable spaxels within the

[1] http://califa.caha.es/DR3

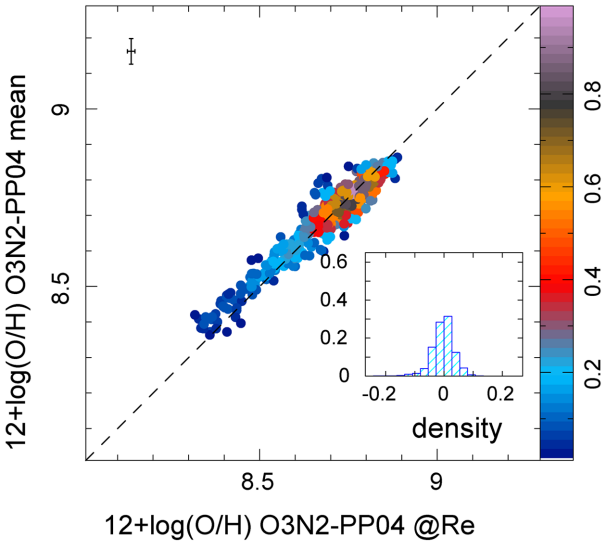

Figure 2. Comparison between the average oxygen abundance across the entire FoV of the data cubes (beyond $\sim 2.5\ r_e$) and the characteristic oxygen abundance at the effective radius using the linear regression technique described in the text. Each solid circle corresponds to an individual galaxy, with a colour code indicating the density of points normalized to the peak density. The upper left error bar indicates the median error estimated for each parameter. The inset shows a histogram of the difference between the two estimations of the oxygen abundance.

FoV of the data cubes (i.e. those ones compatible with being ionized by star formation), and the characteristic abundance derived at the effective radius for a particular oxygen abundance calibrator of the ones described in Section 3.1 (a similar comparison for the remaining calibrators is included in Appendix A). As already noticed by Sánchez et al. (2013), the characteristic abundance is very good representation of the average abundance of a galaxy, with a correlation following the one-to-one relation, and dispersion of ∼0.03 dex. However, the typical error for the characteristic abundance is, on average, a factor two lower than that of the mean oxygen abundance, as shown in Fig. 2.

3.1 Abundance calibrators

Accurate abundance measurements for the ionized gas in galaxies can be derived from metal recombination lines without requiring to know the electron temperature (T_e), since they have a similar temperature dependence to the hydrogen recombination lines (e.g. Bresolin 2007). A major advantage of this method is that they are also insensitive to the temperature fluctuations, characterized by the so-called t_2 parameter (e.g. O'Dell, Peimbert & Peimbert 2003). However, those lines are extremely weak or they are not accessible in the optical wavelength range, in most of the cases (Bresolin 2007), in particular for low-resolution spectroscopy ($R \sim 1000$).

A slightly better approach is to determine the electron temperature (T_e) from the ratio of auroral to nebular line intensities, such as [O III] λ4363/[O III] λλ4959,5007 (Osterbrock 1989). However, this procedure, known as the 'Direct Method', can be affected by electron temperature fluctuations. Even more, as the metallicity increases, the electron temperature decreases due to the cooling by metals and the auroral lines eventually become too faint to measure (e.g. Marino et al. 2013). This same effect makes the strongest oxygen line ratio, $R23 = ([\mathrm{O\,II}]\ \lambda3727 + [\mathrm{O\,III}]\ \lambda4959,5007)/\mathrm{H}\beta$, to be bi-valuated.

It is still under debate which of both procedures derives a more accurate estimation of the oxygen abundance. While it is broadly accepted that the temperature fluctuations would affect our measurements based on the second method (e.g. Peimbert & Peimbert 2006), recent results indicate that the oxygen abundances derived using it agree much better with the value derived from high precision stellar spectroscopy (Bresolin et al. 2016). In any case, both methods require high accurate measurements of the emission line intensity of extremely faint emission lines.

For this reason, in most of the cases they are used calibrators based on strong emission lines, first proposed by Pagel et al. (1979) and Alloin et al. (1979) (see López-Sánchez et al. 2012, for a review). All those calibrators attempt to derive the oxygen (and nitrogen in some cases) abundance based on a known relation between a particular strong-line ratio (or a set of them) and the required abundance. Such relations could be derived using two different approaches: (i) by comparing the known abundances of a set of H II regions with the measured line ratio (or ratios), or (ii) by comparing the line ratios predicted by photoionization models for a set of modelled H II regions, with the input abundances included in those models. Both procedures produce two different families of abundance calibrators, those anchored to the 'Direct Method' and those anchored to photoionization models. It is a well-known and long standing issue that both families of abundances calibrators derive different results (e.g. Kehrig et al. 2008; Morisset et al. 2016). In general, the former ones derive abundances 0.2–0.3 dex lower than the later ones, for the larger abundance values (see Pérez-Montero 2014, for a counter example).

There is a long standing discussion on the nature of this discrepancy. Those supporting the 'Direct Method' approach claim that it is the method with less number of assumptions, being based on basic atomic physics and very few assumptions on the ionization conditions (e.g. Pilyugin, Vílchez & Thuan 2010). They criticize the photoionization models for two main reasons: (i) they are based on strong assumptions on the physical behaviour of atmospheres of the ionizing population (largely unknown) and the structure of ionized nebulae (shape, density distribution...), and (ii) they cannot derive the oxygen abundance without assuming strong correlations, or trends, between this parameter and the ionization strength (e.g. Pérez-Montero 2014), and/or the N/O and S/O relative abundances (e.g. Kewley & Dopita 2002; Dopita et al. 2013). In some cases, those relations are not imposed, but they are implicit, despite the fact that they are not introduced as a prior in the derivation of the abundances (e.g. Blanc et al. 2015). The reason is the strong relation between metal abundance, star effective temperature and blanketing, and between them and the ionization strength that implies a correlation even if it is not imposed. That correlation was already known or hinted since decades (e.g. Evans & Dopita 1985), and it was recently revisited by Sánchez et al. (2015). In summary, by adopting a particular library of ionizing stars it is assumed a particular correlation between oxygen abundance and ionization strength (e.g. Vilchez & Pagel 1988; Morisset et al. 2016).

On the other hand, those supporting the photoionization model calibrators claim that the abundances derived by the Direct Method are far too low for being real (e.g. Blanc et al. 2015), since they can hardly reproduce supersolar oxygen abundances. It is frequently claimed that the fact that the abundances estimated using photoionization models are in a better agreement with the values measured using recombination lines is an indication that it is more accurate to use photoionization models in this regime (e.g. Maiolino

Table 1. Fitting parameters for the MZ relation and its scatter for the set of abundance calibrators used in this study. For each calibrator we list: the standard deviation of the original distribution of the oxygen abundances [$\sigma_{\log(O/H)}$]; the parameters a and b from the fitting of equation (1) to the MZ relation; σ MZ-res lists the standard deviation of the residuals after subtracting the best fit to the MZ relation; the parameters α and β represent the linear fitting of the residuals of the MZ relation with respect to the SFR (see Section 4.2); $\sigma\Delta$ MZ-res lists the standard deviation of the residuals of the linear fitting using the above parameters. We included the third decimal in the σ to highlight any possible difference, however below the second decimal it is totally insignificant.

Metallicity indicator	$\sigma_{\log(O/H)}$ (dex)	MZ best fit		σ MZ-res (dex)	ΔMZ best fit		σ ΔMZ-res (dex)
		a (dex)	b [dex/log ($M_\odot$)]		α (dex)	β [dex/log ($M_\odot$ yr^{-1})]	
O3N2-M13	0.077	8.53 ± 0.04	0.003 ± 0.037	0.060	-0.02 ± 0.01	-0.007 ± 0.005	0.061
PP04	0.111	8.76 ± 0.06	0.005 ± 0.037	0.087	-0.02 ± 0.01	-0.011 ± 0.007	0.088
N2-M13	0.080	8.53 ± 0.04	0.004 ± 0.023	0.060	-0.01 ± 0.01	-0.013 ± 0.005	0.058
ONS	0.095	8.55 ± 0.04	0.006 ± 0.023	0.082	-0.01 ± 0.01	-0.004 ± 0.008	0.082
R23	0.075	8.54 ± 0.03	0.003 ± 0.020	0.065	-0.01 ± 0.01	-0.014 ± 0.009	0.064
pyqz	0.183	9.00 ± 0.12	0.007 ± 0.061	0.147	0.01 ± 0.01	0.086 ± 0.015	0.145
*t*2	0.076	8.85 ± 0.01	0.007 ± 0.001	0.064	0.00 ± 0.00	0.006 ± 0.004	0.063
M08	0.107	8.72 ± 0.10	0.004 ± 0.057	0.087	-0.01 ± 0.01	0.003 ± 0.001	0.087
T04	0.145	8.92 ± 0.04	0.008 ± 0.029	0.133	0.01 ± 0.01	0.014 ± 0.016	0.133
EPM09	0.062	8.59 ± 0.03	0.001 ± 0.017	0.060	-0.01 ± 0.01	-0.001 ± 0.006	0.060
DOP16	0.249	8.86 ± 0.19	0.008 ± 0.094	0.183	-0.01 ± 0.02	0.041 ± 0.023	0.186

et al. 2008). That claim has led to mixed calibrators, like the one presented by Pettini & Pagel (2004) or Maiolino et al. (2008). Those ones anchor the abundances below 12+log(O/H) $\sim$ 8.3 to estimations based on the Direct Method and above that value to estimations based on the photoionization models. However, the argument has a logic flow, since the discrepancy between the measurements based on recombination lines and those based on the Direct Method are supposed to be due to inhomogeneities in the electron temperature, which in general are not included in photoionization models (a priori). Thus, if the values derived using the Direct Method should be corrected by the t_2 effect then, the values derived by photoionization models should be corrected too, since they predict very low values for the t_2 (Peimbert & Peimbert 2006). Therefore, the discrepancy with the values estimated using recombination lines holds, but in the opposite direction.

In order to minimize the effects of selecting a particular abundance calibrator on biasing our results and explore in the most general way the shape of the MZ relation, we have not restricted our analysis to a single calibrator. We derive the abundance using (i) calibrators anchored to the 'Direct Method', including the O3N2 and N2 calibration proposed by Marino et al. (2013, O3N2-M13 and N2-M13 hereafter), the R23 calibration proposed by Kobulnicky & Kewley (2004) as described in Rosales-Ortega et al. (2011), modified to anchor the abundances to the Direct Method (R23 hereafter, Sánchez et al., in preparation), the calibrator proposed by Pilyugin et al. (2010) (ONS hereafter), and a modified version of O3N2 that includes the effects of the nitrogen-to-oxygen relative abundance proposed by Pérez-Montero & Contini (2009) (EPM09 hereafter); (ii) a t_2 correction proposed by Peña-Guerrero, Peimbert & Peimbert (2012) for an average of the abundances derived using the four previous methods, that produce in general very similar results within the nominal errors (T2 hereafter); (iii) two mixed calibrators, based on the O3N2 indicator (Pettini & Pagel 2004, PP04 hereafter) and the R23 indicator (Maiolino et al. 2008, M08 hereafter); and finally (iv) three calibrators based on pure photoionization models, the one included in the PYQZ code, that uses the O2, N2, S2, O3O2, O3N2, N2S2 and O3S2 line ratios as described in Dopita et al. (2013) (pyqz hereafter); a recent calibrator proposed by Dopita et al. (2016) that uses just the N2/S2 and N2 line ratios (DOP16 hereafter); and finally the one adopted by in their exploration of the MZ relation based on the R23 line ratio (T04 hereafter). The complete list of calibrators is included in Table 1.

This selection of calibrators is by no means complete, and it is clearly out of the scope of this article to analyse the similarities and differences between them, both in the final estimated value for the abundances and in the physical assumptions behind them. With the current selection, we try to cover a wide range of possible calibrators, mostly motivated to explore if there is a significant change on the main conclusions depending on the adopted one. The complete list of characteristic oxygen abundances, stellar masses and SFRs are included in Appendix B.

4 RESULTS

Once derived the integrated stellar masses, SFRs and the characteristic oxygen abundance for all the 612 galaxies, we explore the shape of the MZ relation and its possible dependence with the SFR. We start by characterizing the shape of the MZ relation.

4.1 The MZ relation

In Fig. 3, we plot the average abundances at different stellar mass bins for our set of calibrators, together with the individual values for the PP04 calibrator. It is remarkable that almost all abundances follow a similar trend despite of the fact that the different calibrators are based on different assumptions and using different line ratios as indicators. Oxygen abundance increases with the stellar mass for $M > 10^{9.25}\,M_\odot$, reaching an asymptotic value for more massive galaxies, as described by Pilyugin et al. (2007) (the *equilibrium* value in the nomenclature of Belfiore et al. 2015). For masses below $M < 10^{9.25}\,M_\odot$, we have a large dispersion and little statistics. The absolute scale of the relation presents a dependence on the adopted calibrator. In general, calibrators based on photoionization models have a larger dynamical range what is reflected in the larger values for the standard deviation of the oxygen abundances shown in Table 1, and higher abundances. In contrast, calibrators anchored to the Direct Method have a smaller dynamical range (thus, smaller standard deviations), with mixed calibrators lying in between. We also notice that the dispersion around the mean values for the different mass bins is considerably larger for calibrators based on photoionization models than for the rest. As expected, the T2 correction shifts the abundances based on the Direct Method towards values more similar to those derived using photoionization models, but at slightly lower abundances, in general,

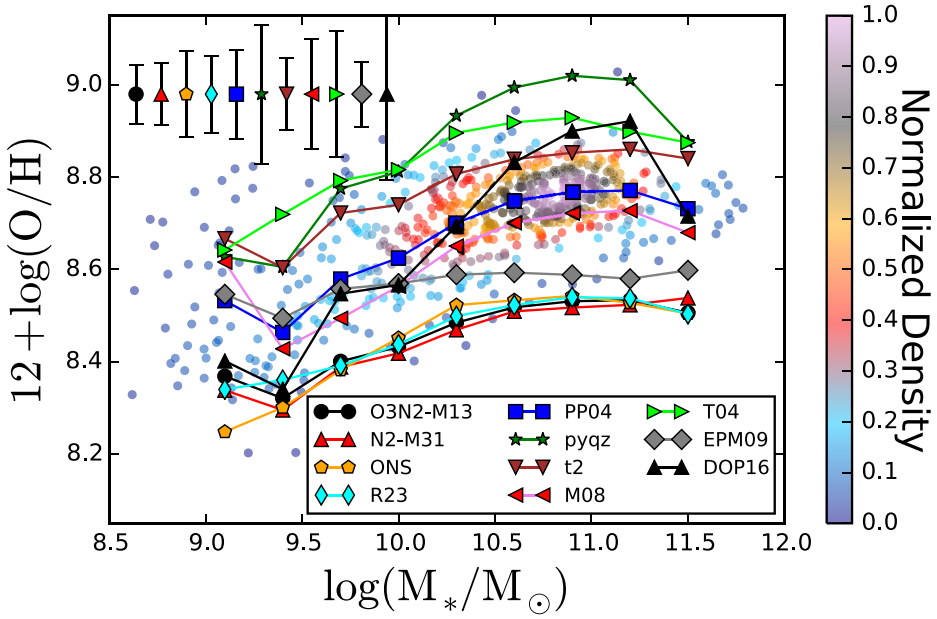

Figure 3. MZ relation derived using different oxygen abundance calibrators for the 612 galaxies extracted from the final CALIFA sample analysed in this article, for the abundances measured at the effective radius (Reff). Coloured solid symbols indicate the distribution for the individual galaxies when adopting the PP04 calibrator, with the colour code indicating the density of points (magenta indicating larger density and light-blue indicating lower density). Line-connected symbols represent median values at a given mass bin for the different calibrators, as indicated in the inset. The error bars in the top-left symbols represent the average standard deviation for each indicator with respect to the median value at different mass bins. A description of the different calibrators is included in Section 3.1.

and a much smaller dispersion around the mean value for each mass bin.

To characterize the MZ relation, we fit the median values at different mass bins using the functional form between these two parameters introduced by Moustakas et al. (2011) and used by Sánchez et al. (2013), for each calibrator:

$$y = a + b(x - c)\exp[-(x - c)] \quad (1)$$

where $y = 12 + \log(\mathrm{O/H})$ and $x = \log(M_*/\mathrm{M}_\odot) - 8.0$. This functional form has been motivated by the shape of the relation (Sánchez et al. 2013). The fitting coefficients, a, b and c represent the asymptotic metallicity, the curvature of the relation and the stellar mass where the metallicity reaches its asymptotic value. We fix $c = 3.5$ since for all the calibrators the asymptotic value is reached at $\log(M_*/\mathrm{M}_\odot) \sim 11.5$. This value was the one reported by Sánchez et al. (2013), and therefore, by adopting it we can perform a direct comparison on the results. However, we should stress that using another value (like $c = 4$, adopted by Barrera-Ballesteros et al. 2017), or fitting this parameter without any restriction does not change the main conclusions of this analysis. It will modify the numerical value of the b parameter, but neither the general shape of the relation nor the dispersion around this relation. In Table 1, we list the best-fitted parameters for the different calibrators. As expected from Fig. 3, T_e-based calibrators show lower values of the asymptotic metallicity, in general. The curvature does not depend strongly on the adopted calibrator, agreeing in all the cases within the errors, that are considerably large in any case.

The value reported for the curvature by Sánchez et al. (2013) was slightly larger ($b = 0.018$) than the one found in here for the same calibrator (PP04, $b = 0.005$). This discrepancy is due to the limited sampling of the MZ relation at low mass in that article. They explore only 1/4 of the full CALIFA sample (150 objects, i.e. the objects observed at that date), and only six of them have a stellar mass lower than $10^{9.5}$ $\mathrm{M}_\odot$, in contrast with the current sample that contain 78 of such galaxies (a substantial number of them due to the CALIFA-extended sample). This difference highlights the importance of revisiting the MZ relation with this larger sample. On the other hand, the asymptotic metallicity ($a = 8.74 \pm 0.01$ dex) agrees within the errors with the currently reported one, and the c parameter was chosen to match the value reported by Sánchez et al. (2013), and therefore they are equal by choice.

We obtain the standard deviation along the MZ relation [$\Delta \log(\mathrm{O/H})$] for each of the calibrators by subtracting the individual metallicities measured for the 612 galaxies by the best-fitted curve. This standard deviation, derived for each calibrator, is a measurement of the scatter around the estimated relation. The results of this analysis are listed in Table 1 as σ MZ-res. These values agree with the size of the error bars shown in Fig. 3, which indicates that the introduction of this particular functional form does not produce any significant effect in the derivation of the scatter around the mean values at each mass. As expected from the previous discussion, the abundances anchored to the Direct Method present a considerable lower dispersion (∼0.05–0.06 dex), in comparison to those based on photoionization models or mixed calibrators (∼0.13–0.18 dex). This difference in the scatter of the MZ relation suggests that mixed or model-based calibrators may introduce an artificial higher dynamical range of the residuals in comparison to the T_e-based ones, which nature should be explored.

To explore the possible dependence of these results on the currently adopted functional form to describe the shape of the MZ relation, we repeated the analysis using a fourth-grade polynomial function (following Mannucci et al. 2010). We found similar standard deviations in the scatter as those reported in Table 1. Indeed, if we had adopted a pure spline interpolation using the mean values included in Fig. 3, we would have found similar results. All these

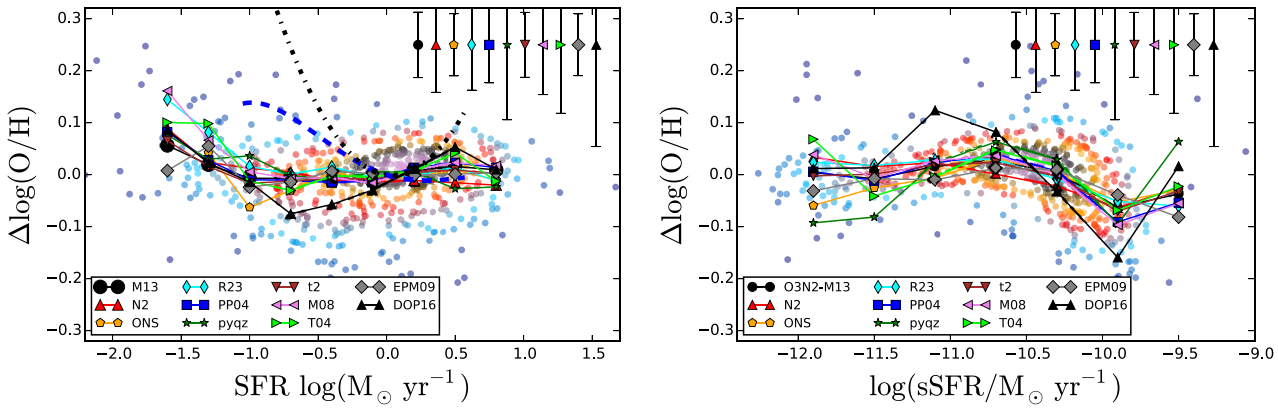

Figure 4. Residuals of the MZ relations from the different analysed calibrators against the SFR (left-hand panel) and the sSFR (right-hand panel). The coloured solid circles correspond to the values derived using the PP04 calibrator, and the line-connected symbols correspond to median values for each bin and calibrator, following the notation presented in Fig. 3. The error bars in the top-right represent the mean standard deviation of the residuals along the considered bins. The blue-dashed line represents the relation between the residuals and the SFR expected when using the secondary relation proposed by Mannucci et al. (2010), and the black-dotted line represents the same relation when adopted the secondary relation proposed by Lara-López et al. (2010).

tests indicate that the scatter around the mean relation does not depend significantly in the adopted functional form.

4.2 Dependence of the MZ residuals with the SFR

To explore if it is needed to introduce a secondary relation with the SFR, we study the possible dependence of the residual of the MZ relation with this parameter, and if the introduction of this dependence will reduce the scatter around the new proposed relation. Any secondary relation that does not reduce the scatter is, based on the Occam's razor, not needed.

Fig. 4 shows, for each calibrator, the residual of the metallicity, once subtracted the estimated MZ relation [Δ log (O/H)] as a function of the SFR and the sSFR for the PPO4 calibrator. In both cases, we present the median values in bins for all the analysed calibrators. For the SFR, we adopt bins of 0.3 log ($M_\odot$ yr^{-1}) width in a range of -1.8 and 0.8 log ($M_\odot$ yr^{-1}). For the sSFR, we adopt bins of 0.4 log ($M_\odot$ yr^{-1}) width in a range of -12.1 and -9.4 log ($M_\odot$ yr^{-1}). The bin sizes and ranges were selected to have the same number of objects in each bin for both the SFR and the sSFR diagrams.

There is a considerable agreement in the median residuals for most of the calibrators along the considered range of SFR and sSFR that all cases are statistically compatible with a zero value. The largest differences are found for the lowest values of SFR [log (SFR) < -1.5], although it does not seem to be statistically significant. For galaxies lying in the SFMS, this SFR corresponds to stellar masses of the order of 10^9 $M_\odot$ (e.g. Cano-Díaz et al. 2016), a range where our sample is not very populated. In general there is no clear trend of the residuals with neither the SFR nor the sSFR. The only two calibrators that present a possible change with both parameters are pyqz and DOP16. However, in none of them there is a clear pattern of increasing or decreasing with the SFR, but just a fluctuation around the zero value. Moreover, we must note that these two calibrators are the ones presenting the larger error bars in the median values.

To compare with the predictions based on the two main proposed functional forms for the secondary relation with the SFR (Lara-López et al. 2010; Mannucci et al. 2010), we overplotted them on top of our data. Following the prescriptions by Mannucci et al. (2010), we build the blue-dashed curve by subtracting their relation without SFR dependence (i.e. μ_0 in their equation 4) to the same relation with SFR dependence (i.e. $\mu_{0.32}$ in their equation 4). In the same way, we build the black-dotted curve by solving the oxygen abundance in equation 1 of Lara-López et al. (2010), and subtracting the MZ relation derived by the same authors (a pure second order polynomial function, described in their section 3). In both cases, we took into account the differences in the IMF of the derived stellar masses, and we considered that SFR galaxies are located along the SFMS, following the functional form proposed by Cano-Díaz et al. (2016). The final plots highlight the fact that the secondary relation of the SFR is more evident at low stellar masses (see fig. 1 of Mannucci et al. 2010). This is observed in our plot. There is a clear inverse relation of the SFR and the scatter in metallicity for SFR <1.0 $M_\odot$ yr^{-1} (shown for the considered calibrator, but observed in all of them). For larger SFRs, the scatter is much smaller, dropping from $\sim$0.08 to $\sim$0.04 dex. In neither of both cases, we can reproduce the predicted trends, although in the case of the Mannucci et al. (2010) relation the residuals match for the range of large masses, where the authors show that the introduction of a secondary relation with the SFR produces no significant effect, in any case.

Despite of the fact that we find no clear trend with the SFR, we attempt to quantify the possible relation of the residuals by performing a linear fitting with the SFR for the different considered calibrators. Table 1 shows the results of this analysis, including the best-fitted parameters (α and β for the zero-point and slope, respectively), together with the standard deviation of the sample of points once removed this possible linear relation (σ ΔMZ-res). The zero-point of the relation is compatible with zero for all the considered calibrators, and the slope for most of them. Only in the case of the pyqz calibrator we find significant positive slope, which points towards a trend opposite to the one reported in previous proposed dependences with SFR. However, when we analyse the residual after taking into account this secondary relation in all of them there is no decrease in the dispersion, even for the pyqz calibrator. Thus, the secondary relation does not produce any improvement.

4.3 Exploring the FMR in detail

In the previous section, we have shown that the residuals of the MZ relation derived using a set of different calibrators for the analysed galaxies do not present any clear trend with neither the SFR nor the sSFR, at least for stellar masses larger than $M > 10^{9.5}$ $M_\odot$.

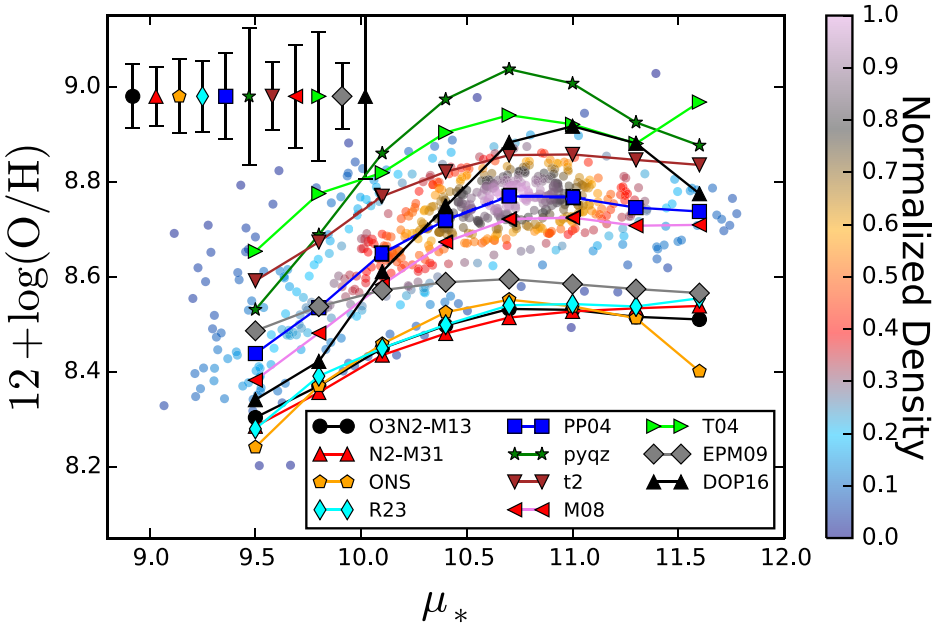

Figure 5. Proposed FMR relation using different metallicity calibrators for the 612 galaxies extracted from the CALIFA final sample analysed in this study. All symbols are similar to the ones shown in Fig. 3.

Table 2. Best-fitted parameters for the $\mu_* Z$ relation, adopting the numerical value for the dependence with the SFR reported by Mannucci et al. (2010) ($d = -0.32$, in equation 2), and the $\mu_{*,\mathrm{d}} Z$ relation, fitting the parameter d (equation ??). For each calibrator, we list the parameters a and b from the fitting to equation (1) and the σ MZ-res, i.e. the standard deviation of the residuals after subtracting the best fit to the $\mu_* Z$ relation. We include the third decimal in the σ to highlight any possible difference. However, below the second decimal, it is totally insignificant.

Metallicity indicator	$\mu_* Z$ best fit		σ FMR-res	$\mu_{*,\mathrm{d}} Z$ best fit			σ_d FMR-res
	a (dex)	b [dex/log ($\mathrm{M}_\odot$)]	(dex)	a (dex)	b [dex/log ($\mathrm{M}_\odot$)]	d [dex/log ($\mathrm{M}_\odot$ yr^{-1})]	(dex)
O3N2-M13	8.54 ± 0.01	0.011 ± 0.002	0.059	8.54 ± 0.01	0.016 ± 0.003	-0.489 ± 0.108	0.057
PP04	8.78 ± 0.01	0.017 ± 0.002	0.085	8.79 ± 0.02	0.023 ± 0.004	-0.489 ± 0.090	0.082
N2-M13	8.54 ± 0.01	0.013 ± 0.001	0.053	8.54 ± 0.01	0.019 ± 0.003	-0.502 ± 0.087	0.049
ONS	8.56 ± 0.02	0.015 ± 0.002	0.081	8.56 ± 0.02	0.016 ± 0.005	-0.249 ± 0.246	0.080
R23	8.57 ± 0.01	0.014 ± 0.001	0.059	8.57 ± 0.02	0.019 ± 0.004	-0.494 ± 0.148	0.057
pyqz	9.00 ± 0.04	0.022 ± 0.005	0.147	9.00 ± 0.02	0.021 ± 0.005	-0.252 ± 0.124	0.146
*t*2	8.86 ± 0.01	0.013 ± 0.002	0.060	8.87 ± 0.01	0.020 ± 0.003	-0.495 ± 0.090	0.058
M08	8.74 ± 0.01	0.018 ± 0.002	0.086	8.75 ± 0.02	0.026 ± 0.005	-0.565 ± 0.112	0.085
T04	8.94 ± 0.01	0.014 ± 0.002	0.130	8.94 ± 0.02	0.013 ± 0.005	-0.076 ± 0.226	0.130
EPM09	8.60 ± 0.01	0.005 ± 0.001	0.058	8.60 ± 0.01	0.007 ± 0.003	-0.609 ± 0.254	0.057
DOP16	8.90 ± 0.04	0.030 ± 0.004	0.179	8.91 ± 0.02	0.040 ± 0.006	-0.424 ± 0.072	0.173

However, for doing this test we adopted a linear functional form for the proposed secondary dependence with those parameters. We adopted this functional form because it is the simplest one to characterize the shape of the possible dependence. Therefore, in a purist way, our results disagree with a possible *linear* secondary relation with the SFR, i.e. with the functional form proposed by Lara-López et al. (2010).

However, due to the non-linear shape of the MZ relation, it is still possible that our data agree with the functional form proposed by Mannucci et al. (2010), in particular, if it is the dispersion across the SFMS the parameter to take into account for this secondary relation as proposed by Salim et al. (2014). To explore this possibility, we adopted the prescriptions by Mannucci et al. (2010) and estimate the μ_* parameter for our galaxies, defined as

$$\mu_* = \log(M/\mathrm{M}_\odot) + \alpha \log(\mathrm{SFR}) \qquad (2)$$

with $\alpha = -0.32$, and analyse the $\mu_* Z$ relation.

Fig. 5 shows the distribution of oxygen abundances along the μ_* parameter for the PP04 calibrator together with the median values of the abundances for different bins of μ_* for the remaining analysed calibrators (with each bin having a width of $\Delta\mu_* 0.3$ dex, and covering the range between 9.3 and 11.6 dex in μ_*). Like in the case of Fig. 3, there is a considerable agreement between the shapes of the $\mu_* Z$ relation for the different considered calibrators, showing the same patters/differences already highlighted for the MZ relations described in Section 4.1.

We characterize the $\mu_* Z$ relation using the same equation that we used to characterize the MZ relation, i.e. equation (1). The results of the derived asymptotic parameter (a) and curvature (b), together with the standard deviation of the residual once subtracted the best-fitted curve are listed in Table 2. When comparing with the values reported for the MZ relation (Table 1), in general it is found that the asymptotic value does not change within the errors. On the other hand, the curvature increases for all the calibrators, like if the horizontal axis has shrunk. This is expected in general.

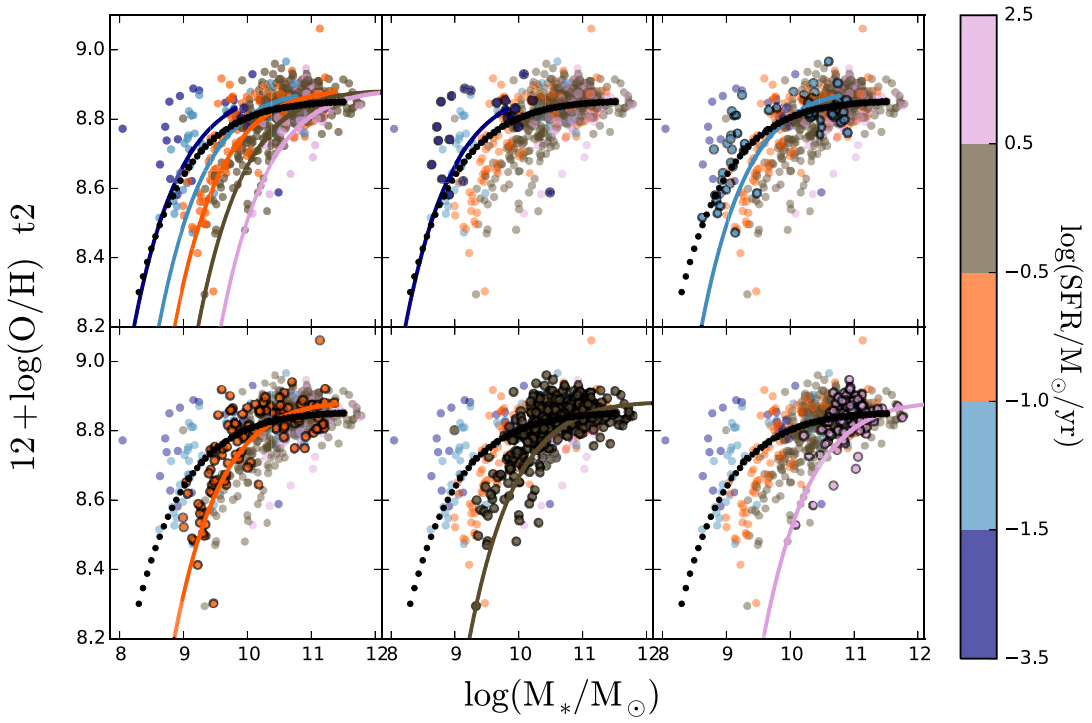

Figure 6. MZ distribution for the *t*2 indicator for the 612 galaxies extracted from the CALIFA final sample analysed in this study. Each galaxy is represented by a solid circle in each panel, with colours indicating the corresponding SFR within each bin indicated in the colourbar. The first panel (top-left) shows the full distribution of galaxies together with the best-fitted $\mu_{*,\mathrm{d}}Z$ relation for the average SFR within each bin, represented as a coloured solid line (equation ??, Table 2). The back dotted line represents the best-fitted MZ relation, without considering any dependence with the SFR (equation 1, Table 1). Each of the remaining panels shows the same distribution highlighting the galaxies and result of the fit for each of the considered SFR bins, from low SFRs (top-middle) to high SFRs (bottom-right).

If the SFR is correlated with the stellar mass following the SFMS, then

$$\log(\mathrm{SFR}/\mathrm{M}_\odot/\mathrm{yr}^{-1}) \sim \alpha \log(M/\mathrm{M}_\odot) \quad (3)$$

where α is of the order of 0.86 (Cano-Díaz et al. 2016). In this case, at a first order $\mu_* \sim 0.72 \log(M/\mathrm{M}_\odot)$, producing a squeeze, what explains the increase of the curvature.

More interesting is the comparison of the standard deviation of the residuals for the μ_*Z relation compared with the MZ one. In general, there is no significant decrease in the standard deviations. In most of the cases the values are equal, or the improvement, if any, affects the third decimal. The largest difference is found for the DOP16 calibrator, with an improvement of $\Delta\sigma = 0.013$ dex in the standard deviation (a reduction of ∼7 per cent in the dispersion). In summary, this analysis shows that the introduction of a secondary relation between the MZ with the SFR using the exact functional form and numerical value of the corrections described by Mannucci et al. (2010) does not produce any significant reduction of the standard deviation of the residuals over the whole distribution.

It is still possible that the adopted functional form for the FMR produces a significant improvement of the MZ relation when considering a different numerical value for the correction of the stellar mass in the formula. We explore that possibility by refitting the data using the following equation:

$$y = a + b(x + \mathrm{d}s - c)\exp(-(x - c)) \quad (4)$$

where y and x are the same parameters described in equation (1) (i.e. the oxygen abundance and the logarithm of the stellar mass), and s is the logarithm of the SFR $s = \log(\mathrm{SFR}/\mathrm{M}_\odot\ \mathrm{yr}^{-1})$. Like in the previous case, we fix parameter c to 3.5 and fit a, b and d. In this formalism, parameter d corresponds to the parameter α described by Mannucci et al. (2010). Hereafter, we refer to that parametrization as the $\mu_{*,\mathrm{d}}Z$ relation. Results are listed in Table 2. In general the best-fitted parameters describe a slightly stronger dependence on the SFR than the one proposed by Mannucci et al. (2010), with values near to the one reported by those authors. The most similar values are reported for the ONS and the PYQZ calibrators, with a value of $d \sim -0.25$. However, in some cases the dependence with the SFR is much weaker (e.g. for the T04 calibrator, where $d = -0.076$). Once more, however, for none of the calibrators, there is a general improvement in the standard deviation of the residuals in the overall distribution.

Fig. 6 illustrates the result of this analysis for one particular calibrator (*t*2). Although similar results are found for the rest of calibrators. We include only one just for clarity. We selected this particular one since it is the one that presents the smaller errors in the derived values for the parameters fitted in equation (1) (Table 1), being one of the three with the smaller dispersion around that relation. In other words, it is one of the calibrators that fits better to the proposed functional form for the MZ relation. Fig. 6 shows the distribution of the oxygen abundance along the stellar mass for five different bins of SFRs together with the location of the best-fitted $\mu_{*,\mathrm{d}}Z$, together with the best-fitted MZ relation (Table 1). Despite of the results listed in Table 2, by eye, it seems that including a secondary relation with the SFR using the functional form proposed by Mannucci et al. (2010) makes the model to match better with the data. The main difference between the MZ relation and the (adjusted) FMR is found at stellar masses lower than $<10^{9.5}$ $\mathrm{M}_\odot$.

Table 3. Comparison of the residuals between the best-fitted $\mu_{*,d}Z$ relation (Table 2) and the MZ relation (Table 1) for the five different star formation bins shown in Fig. 6. We include the range of SFRs covered by each bin, together with the average and standard deviations of the corresponding star formation rates (<SFR>), the residuals of the $\mu_{*,d}Z$ relation and the residuals of the MZ relation. Like in previous tables, we include the third decimal in the σ to highlight any possible difference. However, beyond the second decimal it is totally insignificant. The same comparison was repeated for five different mass bins.

$\log(SFR/M_\odot\ yr^{-1})$ range	<log (SFR)> $\log(M_\odot\ yr^{-1})$	$\mu_{*,d}Z$-res (dex)	MZ-res (dex)
[−3.5, −1.5]	−2.01 ± 0.36	0.062 ± 0.126	0.086 ± 0.122
[−1.5, −1.0]	−1.23 ± 0.15	0.069 ± 0.119	0.015 ± 0.070
[−1, −0.5]	−0.73 ± 0.15	0.042 ± 0.082	−0.022 ± 0.080
[−0.5, 0.5]	0.02 ± 0.28	0.039 ± 0.056	−0.015 ± 0.057
[0.5, 0.5]	0.73 ± 0.16	0.047 ± 0.054	−0.011 ± 0.047
$\log(M_*/M_\odot)$ range	<log (SFR)> $\log(M_\odot\ yr^{-1})$	$\mu_{*,d}Z$-res (dex)	MZ-res (dex)
[8.0, 9.5]	−1.11 ± 0.52	0.117 ± 0.110	−0.022 ± 0.153
[9.5, 10.0]	−0.60 ± 0.42	0.058 ± 0.076	−0.046 ± 0.095
[10.0, 10.5]	−0.18 ± 0.50	0.043 ± 0.068	−0.023 ± 0.072
[10.5, 11.0]	0.05 ± 0.56	0.035 ± 0.049	0.011 ± 0.039
[11.0, 12.5]	0.12 ± 0.57	0.004 ± 0.048	0.006 ± 0.035

However, we should advise against a conclusion guided by visual inspection to the data. Table 3 shows the comparison between the residuals of the best-fitted $\mu_{*,d}Z$ and MZ relations shown in Fig. 6 for the considered star formation bins. Contrary to what the visual inspection may indicate the residuals from the MZ relation have a central value more consistent with the zero with a similar or smaller standard deviations around this central value for all the considered bins up to $\log(SFR) > -1.5\log(SFR/M_\odot\ yr^{-1})$. Below that limit, i.e. the range for which we describe a possible offset in the residuals of the MZ relation along the SFR shown in Fig. 4, the residuals of the central value of these residuals are only 0.024 dex larger than the value derived adopting a dependence with the SFR. This value is well below the 1σ limit ($\sigma \sim 0.12$ dex). Even more, the dispersion around this central value is slightly larger for the $\mu_{*,d}Z$ relation than for the MZ one.

Finally, we repeated the comparison between the two relations shown in Fig. 6 in five mass bins. The results are listed in Table 3. For each mass bin, we include the same parameters: the average SFR at each bin and the average and standard deviations of the residuals once subtracted each of the compared relations. The results of this comparison indicate that including a secondary relation with the SFR does not improve the quality of the MZ relation for stellar masses higher than $>10^{10}$ $M_\odot$. Indeed the standard deviation around the central value is slightly larger and the offset of this central value is of the same order or larger. For the stellar masses below this limit, the dispersion around the central value decreases when taking into account the possible dependence with the SFR. However, the offset of the central value with respect to zero (i.e. the optimal value if the function is a good representation of the distribution) does not decrease significantly. Actually, for the lowest stellar masses this central value is off the zero value, being at $\sim 1\sigma$ from zero.

4.4 Exploring the mass–SFR–Z plane in detail

As we quoted before, Lara-López et al. (2010) introduced the dependence of the oxygen abundance with the stellar mass and the SFR using a totally different approach. Instead of modifying any MZ relation including a term that depends on the SFR, they explored the possibility that the three parameters were distributed along a plane that they called the mass–SFR–oxygen abundance fundamental plane, with the form

$$\log(M_*/M_\odot) = \alpha \log(SFR/M_\odot\ yr^{-1}) + \beta[12 + \log(O/H)] + \gamma \quad (5)$$

finding that the best-fitted parameters were $\alpha = 1.122$, $\beta = 0.474$ and $\gamma = -0.097$. They claim that this relation presents a much smaller scatter (∼0.16 dex) than the MZ relation, that has a standard deviation of 0.26 dex for their data set. Actually, more than modifying the MZ relation, this relation modifies the so-called SFMS, which is a linear relation between the SFR and the stellar mass with a slope of ∼0.8 (e.g. Cano-Díaz et al. 2016, and references therein). By solving the SFR from the equation of Lara-López et al. (2010), it is possible to derive a very similar slope. The novelty of this relation is that they propose that the oxygen abundance should present a linear dependence with the stellar mass once introduced the dependence with the SFR. Solving the oxygen abundance from their equation, the dependence with the other two parameters should be

$$12 + \log(O/H) = a \log(M_*/M_\odot) - b \log(SFR/M_\odot\ yr^{-1}) + c \quad (6)$$

with $a = 2.110$, $b = -2.367$ and $c = 0.205$. Following the same scheme of the previous section, we try to reproduce the results by Lara-López et al. (2010) using our data. We already showed in Fig. 4 that adopting the numerical values for their relation we cannot reproduce our observed data. However, it may still be possible that the actual values of those parameters depend on the adopted calibrator, and therefore we need to find the best-fitted ones for our current data set. For doing so, we fitted equation (6) to our data.

The results from this analysis are listed in Table 4, including for each calibrator the best-fitted parameters and the standard deviation of the residuals once subtracted the model. The comparison of the standard deviation with those listed in Table 1, corresponding to the MZ relation, shows that the introduction of this function does not produce any improvement on the modelling of the data. There is no decrease of the standard deviation for any of the considered calibrators. It is still the case that the residuals are of the same order

Table 4. Best-fitted parameters for M-SFR-Z linear relation, adopting the functional form proposed by Lara-López et al. (2010) (equation 6). For each calibrator, we list the derived parameters a, b and c of the considered equation and the standard deviation of the residuals after subtracting the best-fitted model (σ FP-res). We include the third decimal in the σ to highlight any possible difference. However, below the second decimal it is totally insignificant.

Metallicity indicator	FP best fit a	b	c	σ FP-res (dex)
O3N2	0.10 ± 0.02	−0.020 ± 0.019	8.246 ± 0.051	0.067
PP04	0.14 ± 0.02	−0.028 ± 0.022	8.355 ± 0.061	0.096
N2	0.12 ± 0.02	−0.039 ± 0.018	8.172 ± 0.050	0.065
ONS	0.09 ± 0.03	0.003 ± 0.033	8.264 ± 0.081	0.093
R23	0.11 ± 0.03	−0.037 ± 0.026	8.217 ± 0.067	0.078
pyqz	0.13 ± 0.03	0.054 ± 0.029	8.587 ± 0.077	0.151
*t*2	0.12 ± 0.02	−0.028 ± 0.020	8.511 ± 0.054	0.077
M08	0.14 ± 0.03	−0.049 ± 0.025	8.311 ± 0.073	0.105
T04	0.10 ± 0.03	0.002 ± 0.029	8.626 ± 0.083	0.137
EPM09	0.03 ± 0.02	−0.008 ± 0.019	8.497 ± 0.052	0.069
DP09	0.26 ± 0.03	−0.025 ± 0.032	8.116 ± 0.086	0.187

in both cases. Moreover, by inspecting the reported parameters it is seen that most of the dependence is on the mass ($a \sim 0.1$), with very little contribution of the SFR ($b \sim -0.03$). Indeed, if it is considered a simple linear dependence with the stellar mass the derived standard deviations are very similar to the reported ones. Finally, we would like to highlight that for none of the considered calibrators we can reproduce the very strong dependence of the oxygen abundance reported by Lara-López et al. (2010) with both the stellar mass and the SFR.

4.5 Alternative exploration of the dependence of the MZ relation with the SFR and the sSFR

Salim et al. (2014) proposed a different approach to explore the possible dependence of the MZ relation with the SFR in which the dependence of the Mass of both the oxygen abundance and the SFR are minimized or removed. In this particular case, it is not required to assume a particular functional form for the possible dependence, like in the analysis performed in the previous section. Following these authors, we start selecting only those galaxies that are located along the SFMS. For doing so we use as demarcation line the average between SFMS and the retired galaxies main sequence, proposed by Cano-Díaz et al. (2016), and select only those galaxies for which

$$\log(\mathrm{SFR}/\mathrm{M}_\odot/\mathrm{yr}^{-1}) > -9.58 + 0.835\log(M/\mathrm{M}_\odot). \quad (7)$$

This reduces the sample to 492 pure star-forming galaxies. Then, we remove the dependence of the sSFR with the mass using the SFMS relation in Cano-Díaz et al. (2016), transformed for the sSFR:

$$\Delta\log(\mathrm{sSFR}) = \log(\mathrm{sSFR}/\mathrm{yr}^{-1}) + 8.34 + 0.19\log(M/\mathrm{M}_\odot). \quad (8)$$

This new parameter, the residual of the sSFR across the SFMS, does not include any dependence with the mass by construction, and therefore seems to be promising for detecting any possible correlation of the oxygen abundance with the SFR without the contamination of any relation with the stellar mass.

Fig. 7, top panel, shows the distribution of the oxygen abundance along $\Delta\log(\mathrm{sSFR})$ parameter, including the values for individual galaxies for the PP04 calibrator and the median values in bins of 0.3 dex of the considered parameter. The figure shows that there are clear trends between the oxygen abundance and the $\Delta\log(\mathrm{sSFR})$ parameter, with most of them showing an anticorrelation between both parameters. In general, all calibrators based just on R23 (e.g. R23, T04 or M08), or those that present secondary corrections due to the strength of the ionization (DOP16) show a stronger decrease of the oxygen abundance with the residuals of the sSFR, apparently supporting an FMR dependence with the SFR: the galaxies with more SFR for a certain mass would present a lower oxygen abundance. Finally, there are calibrator for which there is no clear trend (pyqz) or a weak one (ONS). Similar results were found by Salim et al. (2014), who describe a different pattern of the dependence between these two parameters for different calibrators (figs 6 and 7 of that article).

We perform a linear fitting in order to quantify the trends observed in Fig. 7, top panel, and its effect in the dispersion once applied. Results of this analysis are shown in Table 5, including the zero-point and slope of the linear fitting, together with the standard deviations of the distributions after applying the estimated relation. As indicated before, for most of the calibrators there seems to be an anticorrelation between the two parameters. However, when we analyse the effects in the dispersion (by comparing with the original

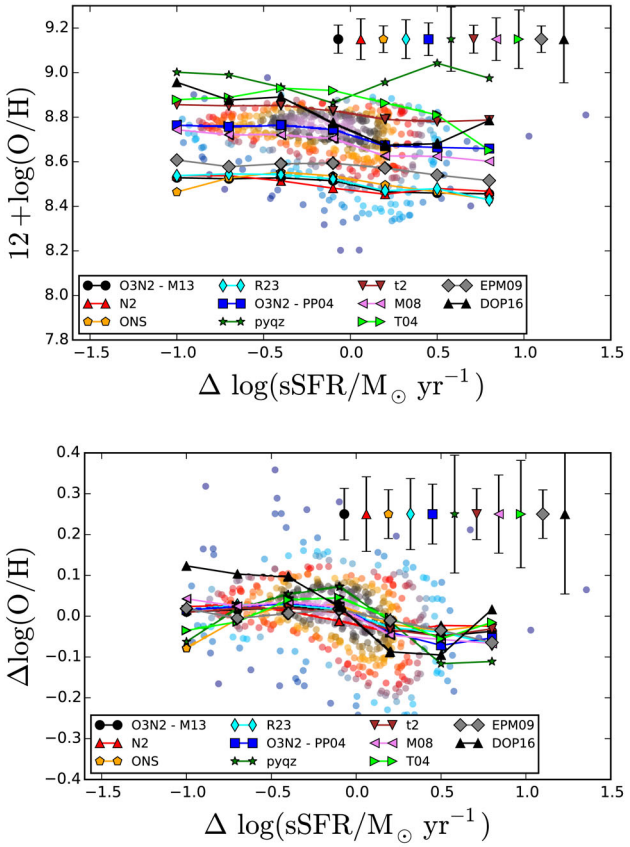

Figure 7. *Top panel:* Distribution of the oxygen abundance along the residual of the sSFR once subtracted the dependence with the stellar mass (i.e. the SFMS), for the individual galaxies (coloured dotted circles) for the PP04 calibrator together with the median oxygen abundance in bins of the residual of the sSFR (line-connected symbols) for the different calibrators. *Bottom panel:* Residual of the oxygen abundance once subtracted the dependence with the stellar mass (i.e. the MR relation), along the residual of the sSFR once subtracted the dependence with the stellar mass, for the individual galaxies (coloured dotted circles) for the PP04 calibrator, together with the median of the residual of the oxygen abundance across the MZ relation in bins of the residual of the sSFR (line-connected symbols) for all the considered calibrators. Symbols are similar to the ones shown in Fig. 4.

Table 5. Results of the analysis of the dependence of the oxygen abundance with the residuals of the sSFR once subtracted the dependence with the mass (i.e. the SFMS), for the different calibrators included in Fig. 7. It is listed the zero-point (α) and the slope (β) from the linear regression, together with the standard deviation of the residuals, once subtracted the derived relation (σ-res).

Metallicity indicator	12+log (O/H) versus Δ log (sSFR) α (dex)	β [dex/log (yr^{-1})]	σ-res (dex)
O3N2-M13	8.48 ± 0.01	−0.04 ± 0.01	0.096
PP04	8.70 ± 0.01	−0.06 ± 0.01	0.140
N2-M13	8.48 ± 0.01	−0.05 ± 0.01	0.103
ONS	8.47 ± 0.02	−0.02 ± 0.02	0.099
R23	8.49 ± 0.01	−0.06 ± 0.01	0.094
pyqz	8.98 ± 0.02	0.01 ± 0.04	0.179
*t*2	8.81 ± 0.01	−0.04 ± 0.01	0.097
M08	8.66 ± 0.01	−0.08 ± 0.01	0.135
T04	8.81 ± 0.03	−0.12 ± 0.05	0.180
EPM09	8.56 ± 0.01	−0.04 ± 0.01	0.073
DOP16	8.77 ± 0.03	−0.13 ± 0.05	0.309

standard deviation listed in Table 1), the introduction of this relation does not improve the dispersion for any calibrator.

The previous analysis is not a test in favour or against any possible secondary relation between the MZ with the SFR or the sSFR. Indeed, it explores a possible primary relation between the oxygen abundance and the dispersion of the sSFR along the SFMS. As indicated before, our results, and that of Salim et al. (2014), show that if there is such a relation, it is less general than the MZ relation, since it depends on the adopted calibrator (not only on the shape, but on the global trend), and it does not decrease the original dispersion as much as the MZ relation itself (compare σ MZ-res parameter from Table 1 with σ-res parameter from Table 5).

To explore if there is a relation of the oxygen abundance with the SFR totally independent of the mass, it is needed to remove that dependence in the two analysed parameters. For doing so, Salim et al. (2014) separated the analysed sample in bins of stellar masses of ∼0.5 dex and performed the same test. When doing so, adopting the O3N2-PP04 on the published CALIFA data up to that date (Sánchez et al. 2013), they found a negative trend in three bins and a positive trend in the remaining one (fig. 10 of that article). However, for the full mass range of the adopted SDSS sub-sample they found a positive trend for all mass bins.

In any case, taking a limited range of stellar masses may reduce the dependence on this parameter, but not remove it completely. Here, we effectively remove that contribution by analysing the possible relations between the residuals of the oxygen abundance once subtracted the MZ relation found for each calibrator [Δ log (O/H), shown in Fig. 4] against the residuals of the sSFR once removed the dependence with the stellar mass [Δ log (sSFR)], for the different calibrators included in this article. Fig. 7, bottom panel, shows this distribution, including the individual points for the O3N2-PP04 calibrator together with the average points for each calibrator in the same bins of Δ log (sSFR) included in the top panel. In this case, there is no general trend for all the calibrators. For some calibrators, like R23, τ2, M08 and EPM09 there is a weak decrease, that it is stronger in the case of DOP16. However, there are calibrators without a clear trend, showing first a rising and then a decrease, like T04, ONS or pyqz. In general, the trends do not seem to have a pattern with the nature of the considered calibrators.

To quantify the dependence between the two parameters and if it has an effect on the dispersion we repeated the analysis described before, performing a linear fitting to the parameters shown in Fig. 7, bottom panel. Table 6 shows the results of this analysis, including the zero-point and slope of the linear fitting, together with the standard deviations of the distributions before and after applying the estimated relation. The different trends described before are now quantified as positive slopes (e.g. ONS), negative ones (e.g. DOP09) or slopes compatible with zero (e.g. T04). More interesting is the comparison between the standard deviations listed in this table with the ones of the original MZ relation, listed in Table 1. In general, there is little change in the dispersion for any of the considered calibrators, and, like in the case of the trend, there is no general pattern. In three cases there is a slight decrease, in all the cases lower than 0.01 dex, and in a similar number of cases there is an increase of the dispersion. Thus, to include a possible secondary correlation with Δ log (sSFR) does not produce any significant general decrease of the dispersion of the MZ relation.

4.6 Dependence of the MZ relation with the SFR

In previous sections, we have explored if the residuals of the MZ relation present an evident correlation with the SFR (Section 4.2), or with the residuals of the SFMS (Section 4.5). We also explored the possible improvements on the relation when introducing two different proposed correlations with the SFR (Sections 4.3 and 4.4). In this section, we actually explore if the parameters of our proposed functional form for the MZ relation (equation 1) present a dependence with the SFR and if taking into account this dependence improves the relation in a significant way. For doing so, we use the same data set used in Section 4.3 and shown in Fig. 6, i.e. the data set comprising the oxygen abundances derived using the *t*2 calibrator split in five different SFR bins (log (SFR/M$_\odot$ yr^{-1})⊂[∞, −1.5], [−1.5, −1], [−1, −0.5], [−0.5, 0.5], [0.5, ∞]). Then, for each subset we derive the best-fitted parameters for equation (1), to see if they present any variation with the SFR. We consider that this approach is more general than assuming a particular functional form for the dependence with the SFR. If the parameters change significantly for each SFR bin, then the shape or the scale of the MZ relation depends on the SFR. However, if the parameters do not present a statistically significant change, then the average MZ relation is a good description of the data, without requiring a secondary dependence with the SFR.

The results from this analysis are shown in Fig. 8 where the best-fitted MZ relations for the different bins of SFR are shown following the same scheme as in Fig. 6. The derived parameters are listed in Table 7, including the central value (mean of the distribution) and standard deviation of the residuals for the best-fitted relation for each SFR range, together with the corresponding values for the full *t*2 data set. For a good fitting, the mean or central value should be near to cero, and the standard deviation should be of the order of the typical error for the oxygen abundance (∼0.3–0.05 dex). Both parameters for the residuals should be compared with the ones listed in the last column of Table 3, that corresponds to the best-fitted MZ relation for the full range of SFRs. For any SFR bin, there is an improvement of the fitting when using the ad hoc MZ relation for each subset in terms of the central value of the residual, that is closer to zero. This is particularly true for the low SFR range [log (SFR/M$\odot$ yr^{-1}) < −1.5]. There is also a slight improvement in the standard deviation, again stronger for the low star formation values. However, we should stress that none of those improvements are statistically significant, and only in the case of the low SFR range the improvement in the central value is near to ∼1σ.

Table 6. Results of the analysis of the dependence of the oxygen abundance residuals with respect to the MZ relation along the residuals of the sSFR once subtracted the dependence with the mass (i.e. the SFMS), for the different calibrators included in Fig. 7. It is listed the zero-point (α) and the slope (β) from the linear regression, together with the standard deviation of the original distribution (σ-org) and that of the residual, once subtracted the derived relation (σ-res).

Metallicity indicator	Δ log (O/H) versus Δ log (sSFR) α (dex)	β [dex/log (yr^{-1})]	σ-res (dex)
O3N2-M13	−0.02 ± 0.01	−0.04 ± 0.01	0.064
PP04	−0.02 ± 0.01	−0.05 ± 0.02	0.093
N2-M13	−0.02 ± 0.01	−0.04 ± 0.01	0.057
ONS	−0.01 ± 0.02	0.04 ± 0.03	0.085
R23	−0.01 ± 0.01	−0.05 ± 0.01	0.063
pyqz	−0.04 ± 0.03	−0.05 ± 0.05	0.153
*t*2	−0.02 ± 0.01	−0.03 ± 0.01	0.064
M08	−0.02 ± 0.01	−0.07 ± 0.02	0.095
T04	−0.01 ± 0.02	−0.02 ± 0.03	0.123
EPM09	−0.02 ± 0.01	−0.03 ± 0.01	0.053
DOP16	−0.03 ± 0.02	−0.15 ± 0.04	0.184

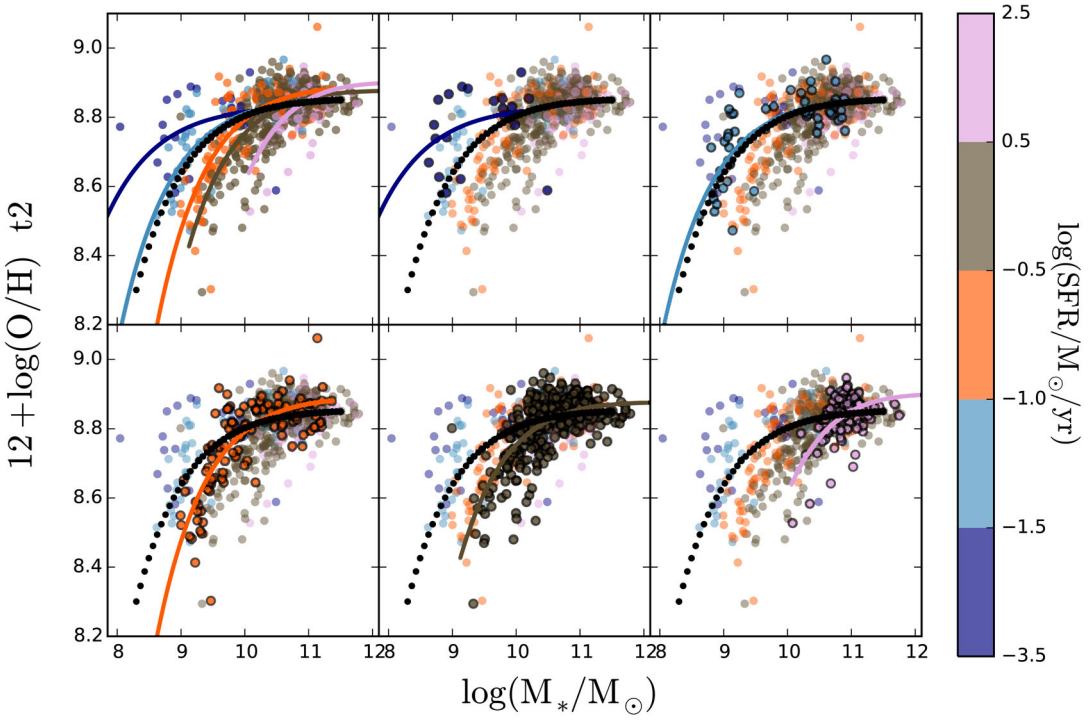

Figure 8. MZ distribution for the *t*2 indicator for the 612 galaxies extracted from the CALIFA final sample analysed in this study. Each galaxy is represented by a solid circle in each panel, with colours indicating the corresponding SFR within each bin indicated in the colourbar. The first panel (top-left) shows the full distribution of galaxies together with the best-fitted MZ relation derived for each bin, represented as a coloured solid line (equation 1, Table 7). The back dotted line represents the best-fitted MZ relation derived for the full data set, without considering any bin in SFR (Table 1). Each of the remaining panels shows the same distributions highlighting the galaxies and results of the fit for each of the considered SFR bins, from low SFRs (top-middle) to high SFRs (bottom-right). For consistency, we adopted the same bins than those shown in Fig. 6.

Table 7. Results of the analysis of the MZ relation for the *t*2 calibrator for the five different star formation bins shown in Fig. 8, already presented in Table 3. We include the range of SFRs covered by each bin, the best-fitted *a* and *b* parameters (equation 1) together with the average and standard deviation of the residuals of the MZ relation. The values for the full range of SFRs have been transcribed from Table 1 to facilitate the comparison. Like in previous tables, we include the third decimal in the σ to highlight any possible difference. However, beyond the second decimal it is totally insignificant.

$\log(SFR/M_\odot\ yr^{-1})$ range	MZ best fit		MZ-res
	a (dex)	*b* [dex/log ($M_\odot$)]	(dex)
[−3.5, −1.5]	8.83 ± 0.12	0.002 ± 0.004	0.003 ± 0.105
[−1.5, −1.0]	8.85 ± 0.05	0.006 ± 0.003	−0.002 ± 0.069
[−1, −0.5]	8.88 ± 0.04	0.013 ± 0.003	0.003 ± 0.070
[−0.5, 0.5]	8.87 ± 0.02	0.017 ± 0.003	0.001 ± 0.049
[0.5, 0.5]	8.88 ± 0.04	0.041 ± 0.025	0.001 ± 0.051
Any SFR	8.86 ± 0.01	0.013 ± 0.002	−0.016 ± 0.060

Regarding the parameters describing the MZ relation, i.e. the asymptotic oxygen abundance (*a*) and the slope of the linear regime (*b*), this analysis indicates that both of them present a weak rising with the SFR. Those trends are similar to the ones described by Mannucci et al. (2010), but including a variation in the asymptotic oxygen abundance that the parametrization presented by those authors did not take into account. Actually, the described trends indicate that the behaviour of the oxygen abundances for low and high stellar masses is different for weak or strong SFRs. While at high stellar masses ($M > 10^{10}$ $M_\odot$) galaxies with low SFR present lower oxygen abundances, at low stellar masses ($M < 10^{10}$ $M_\odot$) the trend is the opposite (being similar for this range to the one described by Maiolino et al. 2008). However, like in the case of the residuals, we should stress that none of those variations seems to be statistically significant. The largest difference is found between the slope of the linear regime for the lowest and highest SFR ranges, being just $\sim 1.5\sigma$ significant. If we take into account the number of galaxies in each bin ($\sim$100), there is a significant difference between the slopes, but they will be at less than 2σ considering the dispersion. Like in the case of the previous tests described in previous sections, there is no statistically significant improvement in the description of the data (i.e. standard deviation of the residuals) when including a possible general variation of the parameters of the adopted MZ relation with the SFR.

5 DISCUSSION

We revisit the MZ relation based on CALIFA data already explored by Sánchez et al. (2013), increasing by a factor four the number of objects (734 objects). These data allow us to derive in a consistent way both the stellar mass and the characteristic metallicity at the effective radius for 612 galaxies. We adopt 11 different abundance calibrators of very different nature to determine in the most general way the shape of the MZ relation and its possible dependence with the SFR. We confirm the reported trend of the MZ relation already shown in many different publications based on both single-aperture spectroscopic surveys (e.g. Tremonti et al. 2004) and IFS ones (e.g. Rosales-Ortega et al. 2012a; Sánchez et al. 2015; Barrera-Ballesteros et al. 2016). Contrary to previous claims (e.g. Kewley

& Ellison 2008), we find that the MZ relation is well represented by the same functional form (i.e. the same shape) irrespectively of the adopted calibrator. The main difference is the value of the asymptotic oxygen abundance at high masses, and in the dispersion around the reported relation. This relation is considerably tighter than the one reported using single-aperture spectroscopy (∼0.1 dex Tremonti et al. 2004), having a dispersion of ∼0.05 dex in the tightest case. This dispersion is of the order of the expected errors for the estimated abundances.

In general, those calibrators anchored to the Direct Method present a tighter correlation with the stellar mass than those ones based on photoionization models. Actually, considering the adopted functional form for the MZ relation, and taking into account that our precision in the derivation of the stellar masses is of the order of ∼0.1 dex, the dispersion around this relation is dominated by the errors in the stellar mass, being the tightest possible even if the oxygen abundance presents no error. If the stellar mass, the integral of the star formation history over cosmic time, is the main driver of the current oxygen abundance in a galaxy, this difference may indicate that indeed photoionization models predict a more imprecise abundance, although the reported value may be more accurate. On the other hand, the calibrators anchored to the Direct Method may produce a more precise value for the oxygen abundance, although its value is more inaccurate. The introduction of a *t*2 correction could be a compromise solution that would make abundances based on the Direct Method more precise and accurate than the ones derived using photoionization models.

We explore different proposed scenarios for a possible secondary relation of the oxygen abundance with the SFR, once considered the main relation of both parameters with the stellar mass. Among them we study: (i) the possible dependence of the residuals of the MZ relation with the SFR, (ii) the effects in the dispersion when imposing one of the most frequently adopted secondary relations (the one proposed by Maiolino et al. 2008) and (iii) the possible relation of the oxygen abundance and the MZ residuals with the specific SFR once removed its dependence with the stellar mass, following Salim et al. (2014). In none of these cases, we find a clear effect (decrease) in the dispersion of the MZ relation for the explored calibrators. We should stress that our sample is not complete/statistically significant for stellar masses below $<10^{9.5}$ $M_{\odot}$.

In addition, we explore in detail the relations between the stellar mass, SFR and oxygen abundances proposed by Maiolino et al. (2008) and Lara-López et al. (2010). In the first case, we find that the parametrization of the possible dependence of the MZ relation with the SFR does produce only a marginal improvement in the accuracy and precision of the relation to describe the data. This improvement, statistically not significant, is larger for the lowest SFR and stellar masses ranges. On the other hand, the parametrization proposed by Lara-López et al. (2010) does not seem to present any improvement over the proposed MZ relation. Finally, we explore the possible dependence of the parameters describing our proposed MZ relation with the SFR, in the most general way. Like in the case of the relation proposed by Maiolino et al. (2008), we find a weak trend with the SFR. However, the behaviour seems to be different for low and high stellar masses. While at low stellar masses galaxies with low SFR seem to have larger oxygen abundances, at high stellar masses they seem to be less metal rich than the average. However, none of those trends seems to be statistically significant and they do not produce a statistically significant improvement of the description of the data compared to an MZ relation independent of the SFR.

These results are totally consistent with the previously reported ones by Barrera-Ballesteros et al. (2017), in which they explored the MZ relation for ∼1700 galaxies extracted from the MaNGA IFS data set. Our results agree both qualitatively and quantitatively, supporting the previous claim by Sánchez et al. (2013) of the lack of a statistically significant secondary relation of the MZ with the SFR for galaxies with stellar masses above $>10^{9.5}$ $M_{\odot}$. We should stress that even using single-aperture spectroscopic data this secondary relation is under discussion. Recently, Kashino et al. (2016) reported that they could not find the proposed secondary relation with the SFR, and Telford et al. (2016) indicated that if it exists it is times weaker than what it was previously claimed. Following Kashino et al. (2016) (in the abstract) we could claim that the fact that we do not find the secondary relation it is not an evidence that it does not exist. Or we could try to understand why in some cases it appears and in others it does not.

The more evident reasons why IFS data consistently fail to reproduce the secondary relation with the SFR of the MZ relation while single-aperture spectroscopic data find it (at different degrees) could be (i) differences in the observational approaches, (ii) differences in the observed samples, (iii) differences in the estimations of the physical quantities (stellar mass, oxygen abundances and SFRs). The first case was explored by Sánchez et al. (2013) in the appendix of that article, in which the effects of selecting a single aperture was reproduced using the CALIFA IFS data. A secondary relation of the same intensity as the one reported by Maiolino et al. (2008) appears in the data when the CALIFA galaxies are randomly shifted to the SDSS redshift range and single-aperture spectra of 3 arcsec/diameter are extracted from the cubes. Therefore, an aperture effect could be one of the primary causes of the discrepancy. More recently Telford et al. (2016) found that there is a significant aperture effect that could produce a secondary relation of the oxygen abundance with the SFR (section 3.3 and fig. 11). However, they discarded that effect without a major reason. In any case, as pointed out, their reported secondary relation is weaker than the one proposed before.

Differences in the observed samples could be a possible source of discrepancy. In the current article and in the recently presented by Barrera-Ballesteros et al. (2016), the number of galaxies is considerably smaller than the one presented in any SDSS based analysis. That could be a potential source of difference if the samples have different properties. However, as shown in Fig. 1, in Sánchez et al. (2013), Walcher et al. (2014) and Sánchez et al. (2016c), the CALIFA sample mimic most of the properties and distributions of the SDSS one, without major biases (for $M_{*} > 109.5$ $M_{\odot}$)

Another reason why there could be different results by different studies is narrowed down in the current analysis (and the one performed by Barrera-Ballesteros et al. 2017): The use of different abundance calibrators. Although our collection of calibrators is far from being complete (look at Padilla & Strauss 2008, for a different collection), we have included the most frequently used ones, covering calibrators with very different natures. In none of them, we have found a clear secondary relation with the SFR. Therefore, to adopt a different calibrator does not seem to be the source of the discrepancy.

The other main reason is the differences in the adopted analysis. In some cases, it was explored the decrease in the dispersion once applied the proposed secondary relation (e.g. Maiolino et al. 2008), or explored the possible systematic effects in the data in detail (e.g. Telford et al. 2016). Finally, in other cases it was proposed a secondary relation without exploring the effects in the dispersion (Salim et al. 2014). Those differences in the methodology may alter the interpretation. In here, we describe negative and positive correlations between the residuals of the MZ relation with the SFR

that in the approach of Salim et al. (2014) may imply a secondary correlation. However, if that correlation does not decrease the initial dispersion, from our perspective it is not required to be introduced.

In any case, the main difference compared with previous studies is the way that the physical parameters are derived. The SFR and the stellar masses are cumulative properties, and therefore they rely on aperture effects as indicated before. In the case of the SFR, it is normally adopted a calibrator based on Hα, corrected by dust attenuation derived by the Hα/Hβ ratio, assuming a certain extinction law (e.g. Kennicutt et al. 1989; Catalán-Torrecilla et al. 2015). However, for single-aperture spectroscopic data it is not possible to disentangle the different ionization sources that may contribute to the Hα flux (Catalán-Torrecilla et al. 2015). This effect is important in low resolution IFS data, as pointed out by Mast et al. (2014), and recently revisited for the MaNGA data set by Zhang et al. (2017). The central region of galaxies may present many different ionization sources and even if the integrated spectra is dominated by star formation, the contribution of other sources, like post-AGBs, shocks or AGNs (e.g. Binette et al. 1994, 2009; Sarzi et al. 2010; Singh et al. 2013; Belfiore et al. 2016; Davies et al. 2016) may be significant and alter the estimation of the SFR. However, recent results indicate that indeed the least presence of an AGN does not alter significantly neither the SFR nor the oxygen abundance and its gradient (e.g. Catalán-Torrecilla et al. 2015; Galbany et al. 2016).

The stellar mass is another source of uncertainties. In many cases, for the SDSS, it is used a stellar mass derived using multiband photometry or the combination of that photometry with the M/L derived from the spectroscopic information. Since the spectroscopic information is biased towards the central regions of the galaxies (although the fraction of light is in average ∼30 per cent at $z \sim 0.1$, at the peak of the SDSS distribution), the M/L may not be representative of the full optical extension. In most of the cases, the uncertainties of the stellar mass are similar or larger than the ones reported for the MZ relation (typically ∼0.1 dex, e.g. Sánchez et al. 2013; González Delgado et al. 2014a; Sánchez et al. 2016b). We consider that the stellar mass derived using IFS should be more accurate and precise, since the M/L is spatially sampled and not averaged, weighting better the low surface brightness disc regions than single-aperture spectroscopic data (that weights more the bulge of galaxies).

Finally for the derivation of the oxygen abundance, the mix of ionization sources could be an important effect in the increase of the dispersion (e.g. Zhang et al. 2017). This is particularly important if we take into account that the abundance is not an integrated property of galaxies, but a relative one that presents clear gradients within the FoV (e.g. Sánchez et al. 2014). Even more if the gradient presents different behaviours at different stellar masses and spatial ranges (Belfiore et al., 2016, 2017; Sánchez-Menguiano et al. 2016). None of these effects can be easily removed by aperture corrections, like the ones proposed by Iglesias-Páramo et al. (2016), and certainly they have not been taken into account in single-aperture spectroscopic studies so far.

In the current article, we adopted as a characteristic abundance for the galaxies the value at the effective radius (that in general is ∼0.05–0.1 dex lower than the central value). In single-aperture spectroscopic surveys, the abundance is dominated by the central values, that, in addition to the possible contamination between different ionization sources, it is not representative of the average oxygen abundance, for the reasons indicated before (mostly due to the drop in the oxygen abundance described for certain galaxies, Sánchez-Menguiano et al. 2016). Therefore, it could still be possible that both results are correct at the same time, and the presence or lack of secondary relation with the SFR is an effect of the region of the galaxy where the abundance is derived. If this is the case, the secondary relation with the SFR found in single-aperture spectroscopic surveys may reflect a local effect in the centre of the galaxies that does not affect the overall evolution of the disc. Indeed, this was discussed in the appendix of Sánchez et al. (2013) as detailed before.

The most widely accepted explanation for the secondary relation with the SFR is the presence of strong outflows connected with the star formation itself that spell metal-rich gas from the galaxy decreasing the oxygen abundance, or reaching an equilibrium abundance (e.g. Belfiore et al. 2016). The lack of a secondary relation with the SFR open new possible interpretations. One of them is that the metal enrichment is dominated by local processes, following the local star formation history, with a MZ relation driven by the local downsizing process (e.g. Pérez et al. 2013; Ibarra-Medel et al. 2016). The almost linear regime of the MZ relation ($M_* < 10^{10}$ M$_\odot$), and its local version, the Σ–z relation ($\Sigma_* < 2.5$ M$_\odot$ pc^{-2}, Rosales-Ortega et al. 2012b), may reflect the regime for which the actual sSFR is stronger, where metal enrichment is still happening. On the other hand, the plateau at larger stellar masses (and mass densities) is conformed by those galaxies (or regions of galaxies) in which bulk of stellar mass was formed in early cosmological times, and thus the enrichment (e.g. more early type spirals or the central regions of disc galaxies). With a star formation regulated mostly by the reservoir of molecular gas and the inflow (e.g. Lilly et al. 2013), both the abundance gradients and the local Σ–z relation are easily reproduced (e.g. Barrera-Ballesteros et al. 2016).

However, this is not the only possible explanation for the shape of the MZ relation. It is possible that the MZ relation has a plateau because it reaches the maximum yield of oxygen abundance, for a characteristic depletion time (Pilyugin et al. 2007). Even more, we still need to accommodate the possible secondary correlations described for the atomic and maybe the molecular cold gas in this picture (Moran et al. 2012; Bothwell et al. 2016), if they are confirmed. A plausible explanation of why there could be a secondary relation with the molecular gas and not with the SFR would be the existence of different depletion times for galaxies at different stellar mass and morphology. It is known that the KS law (e.g. Kennicutt 1998) presents a considerable scatter that it is related with that parameter, and on-going studies indicate that the depletion time may be different for different galaxies and in different regions of the same galaxy (Utomo et al. 2017).

Finally, it may still be possible that outflows affect the chemical evolution of the galaxies more in the central regions than in the outer parts. Like in the case of many other processes, outflows are local processes regulated by the local SFR (and thus the local SN rate), the local gas density, and the local values of the escape velocity and angular momentum. For low-mass galaxies with high star formation, it may be possible to form strong gas outflows (e.g. López-Cobá et al. 2017), that affect the oxygen abundance only in the central regions. Under this scenario, it is still possible that a secondary relation with the SFR is found for the MZ relation for central abundances, and a lack of this secondary relation for the characteristic value. We will explore that possibility in further analyses of the data.

6 CONCLUSIONS

In summary, we cannot confirm the existence of a statistically significant secondary dependence of the MZ relation with the SFR based on our analysis of the characteristic abundance for a sample

of IFS observed galaxies extracted from the CALIFA sample. If there is such secondary relation it is less significant than what it was reported in previous studies, it maybe confined to the low stellar mass range ($M < 10^{9.5}$ $M_{\odot}$) and it does not produce a significant improvement over the MZ relation beyond that mass range. This result agrees with an evolution of the stellar population in galaxies and in particular the metal enrichment dominated by local processes, mostly regulated by the local reservoir of gas, with a limited influence of gas outflows. If the secondary relation is confined to the central oxygen abundances, it may indicate that the effects of outflows or the stopping of the star formation in the central regions modifies the chemical enrichment in those areas in a different way than the general evolution of the discs. However, other possible scenarios are still possible, in particular if the proposed secondary correlations with the atomic and molecular gas are confirmed.

ACKNOWLEDGEMENTS

We thanks the anonymous referee for his/her comments that has helped to improve the manuscript.

SFS and CLC thank the ConaCyt programmes IA-180125 and DGAPA IA100815 and IA101217 for their support to this project. LSM thanks support from the Spanish *Ministerio de Economía y Competitividad* (*MINECO*) via grant AYA2012-31935. LG was supported in part by the US National Science Foundation under Grant AST-1311862. RAM acknowledges support by the Swiss National Science Foundation. SZ has been supported by the EU Marie Curie Career Integration Grant *SteMaGE* Nr. PCIG12-GA-2012-326466 (Call Identifier: FP7-PEOPLE-2012 CIG).

This study uses data provided by the Calar Alto Legacy Integral Field Area (CALIFA) survey (http://califa.caha.es/).

CALIFA is the first legacy survey performed at Calar Alto. The CALIFA collaboration would like to thank the IAA-CSIC and MPIA-MPG as major partners of the observatory, and CAHA itself, for the unique access to telescope time and support in manpower and infrastructures. The CALIFA collaboration also thanks the CAHA staff for the dedication to this project.

Based on observations collected at the Centro Astronómico Hispano Alemán (CAHA) at Calar Alto, operated jointly by the Max-Planck-Institut für Astronomie and the Instituto de Astrofísica de Andalucía (CSIC).

Funding for the Sloan Digital Sky Survey IV has been provided by the Alfred P. Sloan Foundation, the U.S. Department of Energy Office of Science and the Participating Institutions. SDSS-IV acknowledges support and resources from the Center for High-Performance Computing at the University of Utah. The SDSS web site is www.sdss.org.

SDSS-IV is managed by the Astrophysical Research Consortium for the Participating Institutions of the SDSS Collaboration including the Brazilian Participation Group, the Carnegie Institution for Science, Carnegie Mellon University, the Chilean Participation Group, the French Participation Group, Harvard-Smithsonian Center for Astrophysics, Instituto de Astrofísica de Canarias, The Johns Hopkins University, Kavli Institute for the Physics and Mathematics of the Universe (IPMU)/University of Tokyo, Lawrence Berkeley National Laboratory, Leibniz Institut für Astrophysik Potsdam (AIP), Max-Planck-Institut für Astronomie (MPIA Heidelberg), Max-Planck-Institut für Astrophysik (MPA Garching), Max-Planck-Institut für Extraterrestrische Physik (MPE), National Astronomical Observatories of China, New Mexico State University, New York University, University of Notre Dame, Observatário Nacional/MCTI, The Ohio State University, Pennsylvania State University, Shanghai Astronomical Observatory, United Kingdom Participation Group, Universidad Nacional Autónoma de México, University of Arizona, University of Colorado Boulder, University of Oxford, University of Portsmouth, University of Utah, University of Virginia, University of Washington, University of Wisconsin, Vanderbilt University and Yale University.

REFERENCES

Alloin D., Collin-Souffrin S., Joly M., Vigroux L., 1979, A&A, 78, 200
Baldwin J. A., Phillips M. M., Terlevich R., 1981, PASP, 93, 5
Barrera-Ballesteros J. K. et al., 2016, MNRAS, 463, 2513
Barrera-Ballesteros J. K., Sanchez S. F., Heckman T., Blanc G. A., 2017, ApJ, in press
Belfiore F. et al., 2015, MNRAS, 449, 867
Belfiore F. et al., 2017, preprint (arXiv:1703.03813)
Belfiore F., Maiolino R., Bothwell M., 2016, MNRAS, 455, 1218
Binette L., Magris C. G., Stasińska G., Bruzual A. G., 1994, A&A, 292, 13
Binette L., Flores-Fajardo N., Raga A. C., Drissen L., Morisset C., 2009, ApJ, 695, 552
Blanc G. A., Kewley L., Vogt F. P. A., Dopita M. A., 2015, ApJ, 798, 99
Bolatto A. D., Wolfire M., Leroy A. K., 2013, ARA&A, 51, 207
Bothwell M. S., Maiolino R., Kennicutt R., Cresci G., Mannucci F., Marconi A., Cicone C., 2013, MNRAS, 433, 1425
Bothwell M. S., Maiolino R., Cicone C., Peng Y., Wagg J., 2016, A&A, 595, A48
Bresolin F., 2007, ApJ, 656, 186
Bresolin F., Kudritzki R.-P., Urbaneja M. A., Gieren W., Ho I.-T., Pietrzyński G., 2016, ApJ, 830, 64
Brinchmann J., Charlot S., White S. D. M., Tremonti C., Kauffmann G., Heckman T., Brinkmann J., 2004, MNRAS, 351, 1151
Bundy K. et al., 2015, ApJ, 798, 7
Cano-Díaz M. et al., 2016, ApJ, 821, L26
Cardelli J. A., Clayton G. C., Mathis J. S., 1989, ApJ, 345, 245
Catalán-Torrecilla C. et al., 2015, A&A, 584, A87
Cid Fernandes R. et al., 2013, A&A, 557, A86
Cid Fernandes R. et al., 2014, A&A, 561, A130
Croom S. M. et al., 2012, MNRAS, 421, 872
Davé R., Oppenheimer B. D., Finlator K., 2011, MNRAS, 415, 11
Davies R. L. et al., 2016, MNRAS, 462, 1616
Dopita M. A., Sutherland R. S., Nicholls D. C., Kewley L. J., Vogt F. P. A., 2013, ApJS, 208, 10
Dopita M. A., Kewley L. J., Sutherland R. S., Nicholls D. C., 2016, Ap&SS, 361, 61
Duarte Puertas S., Vilchez J. M., Iglesias-Páramo J., Kehrig C., Pérez-Montero E., Rosales-Ortega F. F., 2017, A&A, 599, A71
Ellison S. L., Patton D. R., Simard L., McConnachie A. W., 2008, ApJ, 672, L107
Erb D. K., 2008, ApJ, 674, 151
Erb D. K., Shapley A. E., Pettini M., Steidel C. C., Reddy N. A., Adelberger K. L., 2006, ApJ, 644, 813
Evans I. N., Dopita M. A., 1985, ApJS, 58, 125
Fukugita M., Shimasaku K., Ichikawa T., 1995, PASP, 107, 945
Galbany L. et al., 2016, A&A, 591, A48
Gallazzi A., Charlot S., Brinchmann J., White S. D. M., Tremonti C. A., 2005, MNRAS, 362, 41
García-Benito R. et al., 2015, A&A, 576, A135
Garnett D. R., Shields G. A., 1987, ApJ, 317, 82
Gomes J. M. et al., 2016, A&A, 586, A22
González Delgado R. M. et al., 2014a, A&A, 562, A47
González Delgado R. M. et al., 2014b, ApJ, 791, L16
Henry A. et al., 2013, ApJ, 776, L27
Hughes T. M., Cortese L., Boselli A., Gavazzi G., Davies J. I., 2013, A&A, 550, A115
Husemann B. et al., 2013, A&A, 549, A87
Ibarra-Medel H. J. et al., 2016, MNRAS, 463, 2799
Iglesias-Páramo J. et al., 2013, A&A, 553, L7
Iglesias-Páramo J. et al., 2016, ApJ, 826, 71
Kashino D., Renzini A., Silverman J. D., Daddi E., 2016, ApJ, 823, L24

Kehrig C., Vílchez J. M., Sánchez S. F., Telles E., Pérez-Montero E., Martín-Gordón D., 2008, A&A, 477, 813
Kehrig C. et al., 2012, A&A, 540, A11
Kelz A. et al., 2006, PASP, 118, 129
Kennicutt R. C. Jr., , 1998, ApJ, 498, 541
Kennicutt R. C. Jr.,, Keel W. C., Blaha C. A., 1989, AJ, 97, 1022
Kewley L. J., Dopita M. A., 2002, ApJS, 142, 35
Kewley L. J., Ellison S. L., 2008, ApJ, 681, 1183
Kewley L. J., Dopita M. A., Sutherland R. S., Heisler C. A., Trevena J., 2001, ApJ, 556, 121
Kobulnicky H. A., Kewley L. J., 2004, ApJ, 617, 240
Lara-López M. A. et al., 2010, A&A, 521, L53
Lequeux J., Peimbert M., Rayo J. F., Serrano A., Torres-Peimbert S., 1979, A&A, 80, 155
Lilly S. J., Carollo C. M., Pipino A., Renzini A., Peng Y., 2013, ApJ, 772, 119
López-Cobá C. et al., 2017, MNRAS, 467, 4951
López-Sánchez Á. R., Dopita M. A., Kewley L. J., Zahid H. J., Nicholls D. C., Scharwächter J., 2012, MNRAS, 426, 2630
Maier C., Lilly S. J., Ziegler B. L., Contini T., Pérez Montero E., Peng Y., Balestra I., 2014, ApJ, 792, 3
Maier C., Ziegler B. L., Lilly S. J., Contini T., Pérez-Montero E., Lamareille F., Bolzonella M., Le Floc'h E., 2015, A&A, 577, A14
Maier C. et al., 2016, A&A, 590, A108
Maiolino R. et al., 2008, A&A, 488, 463
Mannucci F., Cresci G., Maiolino R., Marconi A., Gnerucci A., 2010, MNRAS, 408, 2115
Marino R. A. et al., 2013, A&A, 559, A114
Mast D. et al., 2014, A&A, 561, A129
Moran S. M. et al., 2012, ApJ, 745, 66
Morisset C. et al., 2016, A&A, 594, A37
Moustakas J. et al., 2011, preprint (arXiv:1112.3300)
O'Dell C. R., Peimbert M., Peimbert A., 2003, AJ, 125, 2590
Osterbrock D. E., 1989, Astrophysics of Gaseous Nebulae and Active Galactic Nuclei. University Science Books, Mill Valley, CA
Padilla N. D., Strauss M. A., 2008, MNRAS, 388, 1321
Pagel B. E. J., Edmunds M. G., Blackwell D. E., Chun M. S., Smith G., 1979, MNRAS, 189, 95
Peimbert M., Peimbert A., 2006, in Infante L., Rubio M., eds, Rev. Mex. Astron. Astrofis. Conf. Ser., Vol. 26. p. 163
Peña-Guerrero M. A., Peimbert A., Peimbert M., 2012, ApJ, 756, L14
Pérez E. et al., 2013, ApJ, 764, L1
Pérez-Montero E., 2014, MNRAS, 441, 2663
Pérez-Montero E., Contini T., 2009, MNRAS, 398, 949
Pettini M., Pagel B. E. J., 2004, MNRAS, 348, L59
Pilyugin L. S., Thuan T. X., Vílchez J. M., 2007, MNRAS, 376, 353
Pilyugin L. S., Vílchez J. M., Thuan T. X., 2010, ApJ, 720, 1738
Relaño M., Kennicutt R. C. Jr.,, Eldridge J. J., Lee J. C., Verley S., 2012, MNRAS, 423, 2933
Rosales-Ortega F. F., Díaz A. I., Kennicutt R. C., Sánchez S. F., 2011, MNRAS, 415, 2439
Rosales-Ortega F. F., Sánchez S. F., Iglesias-Páramo J., Díaz A. I., Vílchez J. M., Bland-Hawthorn J., Husemann B., Mast D., 2012a, ApJ, 756, L31
Rosales-Ortega F. F., Sánchez S. F., Iglesias-Páramo J., Díaz A. I., Vílchez J. M., Bland-Hawthorn J., Husemann B., Mast D., 2012b, ApJ, 756, L31
Roth M. M. et al., 2005, PASP, 117, 620
Salim S., Lee J. C., Ly C., Brinchmann J., Davé R., Dickinson M., Salzer J. J., Charlot S., 2014, ApJ, 797, 126
Salim S., Lee J. C., Davé R., Dickinson M., 2015, ApJ, 808, 25
Salpeter E. E., 1955, ApJ, 121, 161
Sánchez S. F. et al., 2012, A&A, 538, A8
Sánchez S. F. et al., 2013, A&A, 554, A58
Sánchez S. F. et al., 2014, A&A, 563, A49
Sánchez S. F. et al., 2015, A&A, 574, A47
Sánchez S. F. et al., 2016a, Rev. Mex. Astron. Astrofis., 52, 21
Sánchez S. F. et al., 2016b, Rev. Mex. Astron. Astrofis., 52, 171
Sánchez S. F. et al., 2016c, A&A, 594, A36
Sánchez-Menguiano L. et al., 2016, A&A, 587, A70
Sarzi M. et al., 2010, MNRAS, 402, 2187
Saviane I., Yegorova I., Proust D., Bresolin F., Ivanov V., Held E. V., Salzer J., Rich R. M., 2014, Mem. Soc. Astron. Italiana, 85, 417
Schlegel D. J., Finkbeiner D. P., Davis M., 1998, ApJ, 500, 525
SDSS Collaboration et al., 2016, preprint (arXiv:1608.02013)
Singh R. et al., 2013, A&A, 558, A43
Telford O. G., Dalcanton J. J., Skillman E. D., Conroy C., 2016, ApJ, 827, 35
Tremonti C. A. et al., 2004, ApJ, 613, 898
Utomo D. et al., 2017, preprint (arXiv:1704.03481)
Vila-Costas M. B., Edmunds M. G., 1992, MNRAS, 259, 121
Vilchez J. M., Pagel B. E. J., 1988, MNRAS, 231, 257
Walcher C. J. et al., 2014, A&A, 569, A1
Zhang K. et al., 2017, MNRAS, 466, 3217

SUPPORTING INFORMATION

Supplementary data are available at *MNRAS* online.

published_table.txt

Please note: Oxford University Press is not responsible for the content or functionality of any supporting materials supplied by the authors. Any queries (other than missing material) should be directed to the corresponding author for the article.

APPENDIX A: CHARACTERISTIC VERSUS AVERAGE OXYGEN ABUNDANCES

In Section 3, we indicate that the characteristic oxygen abundance of a galaxy is a good representation of the average oxygen abundance across the entire optical extension of the galaxy, as already noticed by Sánchez et al. (2013). In order to illustrate it, we show the comparison between these two parameters for the galaxies of the current analysed sample for the PP04 calibrator (Fig. 2). Fig. A1 shows a similar comparison for the remaining 10 calibrators discussed along this article. As expected the characteristic and mean oxygen abundances are well distributed along a one-to-one relation for the different calibrators. Even more, it is shown that the typical error for the mean oxygen abundance is systematically larger than the one estimated for the characteristics one. This is expected since the second one is the result of a linear regression using a large number of individual values. In order to quantify how the two parameters compare, we show in Table A1 the mean and standard deviation of the differences between them. We include the third decimal, although it is clearly insignificant, to highlight any possible difference. However, it is evident that both parameters are very

Table A1. Comparison between the average and characteristic oxygen abundances. For each calibrator of the ones discussed in this article, we include the mean and standard deviations of the differences between both parameters for the set of galaxies included in our study.

Metallicity indicator	Δ log(O/H) (dex)	$\sigma_{\Delta\ \log(O/H)}$ (dex)
O3N2-M13	−0.002	0.031
PP04	−0.002	0.045
N2-M13	−0.009	0.033
ONS	0.012	0.049
R23	−0.039	0.051
*t*2	−0.001	0.032
M08	0.010	0.056
T04	−0.017	0.116
EPM09	−0.020	0.047
DOP16	0.014	0.094

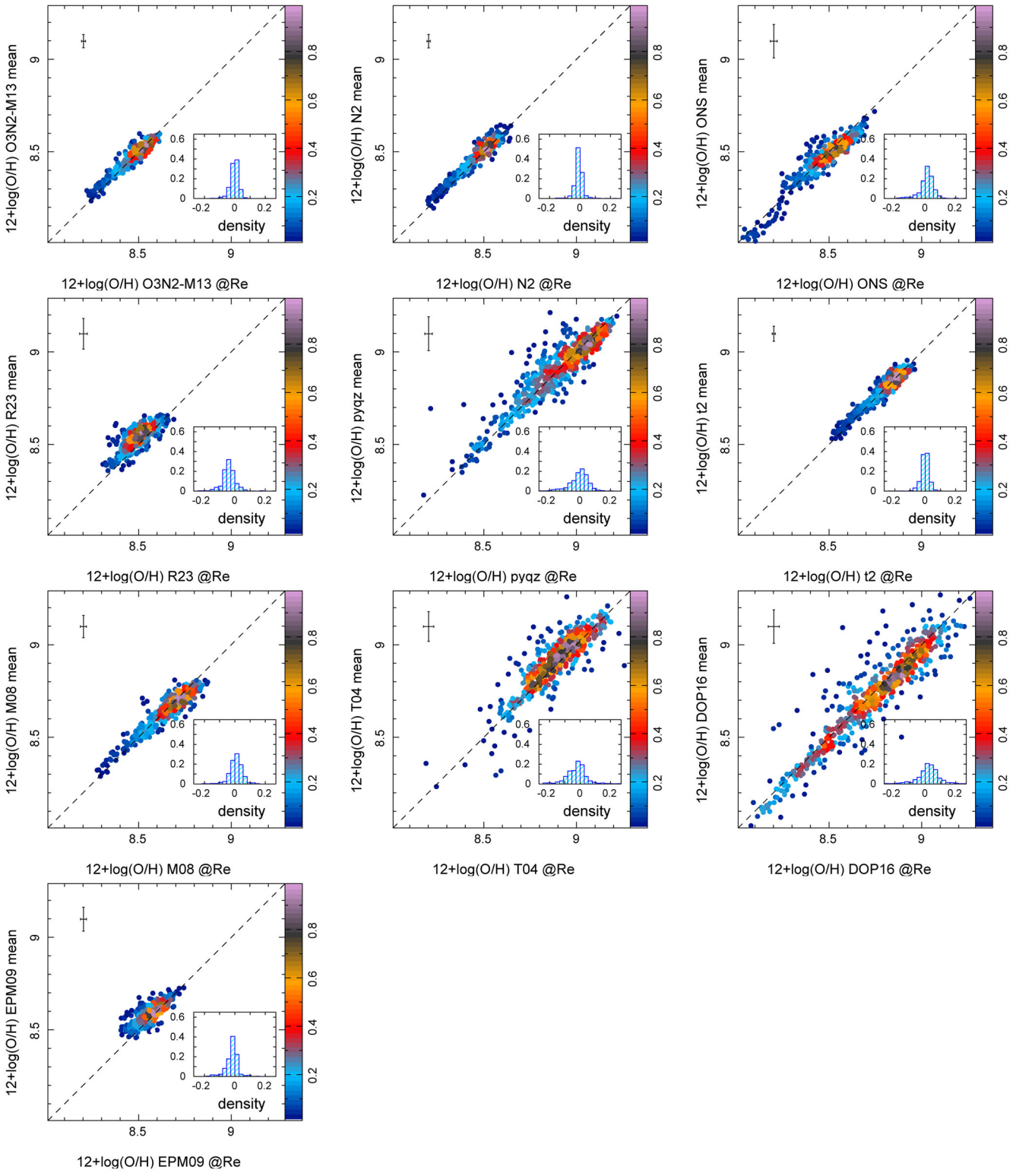

Figure A1. Comparison between the average oxygen abundance across the entire FoV of the data cubes (beyond ∼2.5 r_e) and the characteristic oxygen abundance at the effective radius using the linear regression technique described in the text for the different calibrators discussed in this study. Each panel corresponds to a different calibrator. In each panel, solid circles correspond to the values for an individual galaxy, with a colour code indicating the density of points normalized to the peak density. The error bar indicates the median error estimated for each parameter. The inset shows a histogram of the difference between the two estimations of the oxygen abundance.

similar, with a difference well below the estimated errors. It is important to notice that the matching between the two estimations is not equally good for the different calibrators. In general, those calibrators using a larger number of emission line ratios, or based on high order polynomials of the considered line ratios present a larger disagreement. However, the calibrator with the larger difference is that one based on R23, with an offset of $\sim -0.039 \pm 0.051$ dex.

APPENDIX B: DATASET

Table B1 includes the integrated stellar masses and SFRs for 734 galaxies included in the analysed sample, derived as described in Section 3, together with their nominal errors (i.e. not taken into account systematic errors). For those galaxies for which it was possible to derive the characteristic oxygen abundance using the different calibrators described in Section 3.1, we include each of their corresponding values. When it was not possible to derive a particular oxygen abundance, it is marked with a nan value. The listed errors for the calibrators are the nominal ones derived from the linear regression described in Section 3, and for that reason are considerable smaller than the typical errors derived from single-aperture spectroscopic studies. The systematic errors associated with each calibrator are not listed, although they were taken into account in the analysis of the data. An electronic version of this table can be downloaded from the CALIFA FTP server: ftp://ftp.caha.es/CALIFA/dataproducts/MZ_CALIFA/published_table.csv.

Table B1. Stellar Masses, star formation rates and characteristics abundances for the all the considered calibrators. *The full table is available on-line.*

CALIFA name	$\log(M_*/M_\odot)$	$\log(SFR/M_\odot\ yr^{-1})$	12+log(O/H)					
			O3N2-M13	N2-M13 *t*2	ONS M08	R23 T04	O3N2-PP04 DOP	PYQZ EPM
2MASXJ01331766+1319567	9.38 ± 0.11	−0.94 ± 0.06	8.39 ± 0.02	8.36 ± 0.01 8.69 ± 0.01	8.36 ± 0.01 8.50 ± 0.02	8.47 ± 0.03 8.86 ± 0.04	8.56 ± 0.03 8.34 ± 0.02	8.69 ± 0.01 8.59 ± 0.04
2MASXJ09065870	11.60 ± 0.12	0.41 ± 0.06	8.47 ± 0.06	8.54 ± 0.09 8.83 ± 0.09	nan ± nan 8.65 ± 0.30	8.55 ± 0.50 8.99 ± 0.33	8.68 ± 0.09 8.94 ± 1.20	8.88 ± 0.59 8.51 ± 0.46
2MASXJ09591230	10.39 ± 0.12	−1.03 ± 0.07	nan ± nan	nan ± nan nan ± nan	nan ± nan nan ± nan	nan ± nan nan ± nan	nan ± nan nan ± nan	nan ± nan nan ± nan
2MASXJ12095669	10.48 ± 0.12	−0.84 ± 0.06	8.53 ± 0.09	8.55 ± 0.07 8.85 ± 0.07	nan ± nan 8.67 ± 0.09	8.58 ± 0.12 8.86 ± 0.24	8.77 ± 0.13 8.68 ± 0.38	8.81 ± 0.20 8.66 ± 0.12
2MASXJ15024995+4847010	10.43 ± 0.10	−0.44 ± 0.05	8.47 ± 0.02	8.46 ± 0.05 8.80 ± 0.08	nan ± nan 8.63 ± 0.11	8.45 ± 0.07 8.53 ± 0.38	8.68 ± 0.03 8.68 ± 0.33	8.68 ± 0.09 8.60 ± 0.13
2MASXJ15393305+3205382	11.08 ± 0.10	−0.38 ± 0.06	8.51 ± 0.03	8.57 ± 0.05 8.84 ± 0.05	nan ± nan 8.64 ± 0.06	8.50 ± 0.11 8.88 ± 0.13	8.73 ± 0.05 8.92 ± 0.20	8.93 ± 0.12 8.46 ± 0.16
2MASXJ15570268+3725001	10.15 ± 0.10	−1.35 ± 0.05	8.51 ± 0.06	8.58 ± 0.09 8.87 ± 0.03	nan ± nan 8.68 ± 0.15	8.58 ± 0.14 8.98 ± 0.15	8.74 ± 0.09 8.55 ± 0.56	8.68 ± 0.25 8.66 ± 0.33
2MASXJ16152860	10.06 ± 0.08	−0.61 ± 0.06	8.49 ± 0.08	8.53 ± 0.14 8.80 ± 0.04	nan ± nan 8.69 ± 0.09	8.51 ± 0.24 8.80 ± 0.53	8.71 ± 0.12 8.87 ± 0.67	8.83 ± 0.23 8.58 ± 0.21
ARP180	10.42 ± 0.09	−0.71 ± 0.07	8.46 ± 0.03	8.50 ± 0.04 8.81 ± 0.04	8.43 ± 0.07 8.64 ± 0.07	8.51 ± 0.09 8.65 ± 0.12	8.67 ± 0.04 8.65 ± 0.12	8.76 ± 0.12 8.58 ± 0.06
ARP220	10.86 ± 0.11	1.86 ± 0.06	8.56 ± 0.05	8.67 ± 0.05 8.95 ± 0.03	8.41 ± 0.07 8.74 ± 0.06	8.74 ± 0.30 8.64 ± 0.28	8.81 ± 0.07 9.07 ± 0.18	9.07 ± 0.11 8.57 ± 0.11

This paper has been typeset from a TEX/LATEX file prepared by the author.